FISSION IN EXOTIC NUCLEI USING DENSITY FUNCTIONAL THEORY

By

Zachary Matheson

A DISSERTATION

Submitted to
Michigan State University
in partial fulfillment of the requirements
for the degree of

Physics — Doctor of Philosophy
Computational Mathematics, Science and Engineering — Dual Major

2019

ABSTRACT

FISSION IN EXOTIC NUCLEI USING DENSITY FUNCTIONAL THEORY

By

Zachary Matheson

This is my abstract.

Dedicated to I dunno

ACKNOWLEDGMENTS

I dunno who to acknowledge, either

TABLE OF CONTENTS

LIST OF FIGURES

Chapter 1

Introduction

1.1 History of Fission Theory

Nuclear fission is the fundamental physical process by which a heavy nucleus decays to two smaller nuclei with approximately equal masses, and a proper understanding of fission is critical for applications in reactor physics, nuclear astrophysics, and stockpile stewardship. Fission was first observed by Hahn and Straßmann in 1939 [1] as they bombarded uranium atoms with neutrons and detected barium, but at the time the men could not explain their observations. The explanation came shortly thereafter in letters to the editor by Meitner and Frisch [2] and by Bohr [3]. In Meitner and Frisch's paper they said "On account of their close packing and strong energy exchange, the particles in a heavy nucleus would be expected to move in a collective way which has some resemblance to the movement of a liquid drop. If the movement is made sufficiently violent by adding energy, such a drop may divide itself into two smaller drops…It seems therefore possible that the uranium nucleus has only small stability of form, and may, after neutron capture, divide itself into two nuclei of roughly equal size (the precise ratio of sizes depending on finer structural features and perhaps partly on chance).". A different form of fission, dubbed spontaneous fission because it occurred without bombardment by neutrons or any other projectiles, was reported by Flerov and Petrjak in a single-paragraph letter to *Physical Review* in 1940 [4]. For the remainder of this dissertation,

I will be referring mainly to spontaneous fission unless stated otherwise.

Fission is easy to understand qualitatively but remarkably difficult to explain quantitatively. Theoretically, making predictions about fission is challenging because, thanks to the large number of particles involved and the complex collective interactions which take place when one system deforms and becomes two, fission calculations have an "inextinguishable thirst for computing power," as stated in [5]. One could argue that nuclear fission theory has leapt forward in three major waves.

1.1.1 Liquid Drop Model

The first major wave of nuclear fission theory goes back to the very beginning of the nuclear age, with the liquid drop model in the 1930s. The liquid drop model was developed by Weizsäcker in 1935 [6] as a way of describing the collective properties of nuclei. It was later adapted by Bohr and Wheeler to quantitatively describe nuclear fission in terms of bulk properties of nuclei [7]. This model was able to successfully describe nuclear binding energies and the energetics of nuclear fission.

1.1.2 Strutinsky shell correction approach

The second wave came with Strutinsky's microscopic correction in the late 1960s, which essentially amounted to adding a quantum mechanical correction to the liquid drop energy. This correction, based on the nuclear shell model, is added in order to better account for the added stability that occurs when a nucleus contains a "magic number" of protons and/or neutrons [8–10]. This is necessary, for instance, in order to explain the occurrence of fission fragments of unequal mass. These models go by the name "microscopic-macroscopic"

because they combine the "macroscopic" bulk properties of the liquid-drop model with the "microscopic" quantum mechanical Strutinsky shell corrections.

These microscopic-macroscopic ("micmac") fission models are computationally fairly inexpensive, and can achieve quite satisfactory results. However, since the model is based on a phenomenological description of what is actually a quantum mechanical system, its predictive power is limited, and there is no clear way of making systematic improvements. A more reliable approach would be to consider the individual nucleon states using some kind of quantum many-body method.

1.1.3 Self-consistent models and the supercomputing era

The third major wave is taking place now, heralded by the age of supercomputers. Fission was listed in a recent 2017 report to the Department of Energy [11] as one of the problems which motivates the drive towards exascale computing. For large systems with many, many particles, density functional theory (DFT) is a way to recast the Schrödinger equation involving $\sim$200 particles into a simpler problem involving only a few densities and currents (see section 2.1.1). With DFT as a way of calculating nuclear properties quantum-mechanically, one can then combine self-consistent methods developed over the past several decades with modern high-performance computing platforms to predict fission properties, such as lifetimes and fragment yields. Fortunately, a great deal of work has been done to achieve exactly this (see the review article on self-consistent approaches to fission in [5]). Some of the ideas which are used were inspired by lessons learned from micmac and other, simpler models; others are unique to DFT. Our approach is described in detail in chapter 2.

These advances in computing come simultaneously with advances in accelerator design and technology and other advances which allow experimental nuclear physics to reach far

beyond what has been done before. For instance, the Facility for Rare Isotope Beams (FRIB) at Michigan State University is projected to be able to nearly double the number of isotopes that can be produced synthetically [12]. Together, state-of-the-art facilities for experiment and high-performance computing for theory are expected to lead to rapid advancement in our understanding of atomic nuclei.

1.2 Predicting fission fragments

Microscopic models (as self-consistent models are often called) are increasingly able to predict properties of fission fragments; however, a comprehensive description of fission fragments (including mass and fragment yields, excitation and kinetic energy distributions, angular dependence, spin, neutron emission) in a microscopic framework remains elusive. In Chapter 2 I will discuss two different approaches for describing the characteristics of fission fragments. In either case, the challenge, now, is to do these calculations cheaply. In every theoretical calculation, one must ask oneself "What approximations can I safely make?" and "What are the important degrees of freedom for this problem?" One may also reduce the total time-to-answer via improvements to the computational workflow itself, such as better file handling and parallelization.

A major source of this elusiveness is due to the sheer difficulty of describing a smooth transition from one nucleus to two, a concept which is plagued with ambiguities. How can one precisely identify two distinct fragments when the wavefunctions of one fragment's constituent nucleons may extend into the opposite fragment? And how do those correlations between nucleons affect the energetics of the resulting fragments? We will briefly address these questions as well in Appendix A.

1.3 Goals of the project

By far the most commonly-studied region so far for fission has been the region of actinides near ^{235}U, which includes isotopes of uranium, plutonium, and thorium relevant for nuclear energy/reactor physics and stockpile stewardship/defense. Isotopes in this region tend to fission asymmetrically, with the larger prefragment influenced by the shell structure of ^{132}Sn and resulting in a heavy fragment distribution centered around $\sim^{140}$Te. However, recent experiments have highlighted other forms of fission which take place in other regions of the nuclear chart.

Given the aforementioned recent interest in rare and exotic nuclei, we have applied our model to study spontaneous fission in exotic systems found in other regions of the nuclear chart, with a focus on primary fragment yields. First, in chapter 4 we discuss bimodal fission in the neutron-deficient isotope platinum-178, which until recently was expected to fission symmetrically. This region is a good one in which to test fission models because of the large isospin asymmetry ($N/Z \approx 1.3$, compared to $N/Z \approx 1.5$ near the valley of stability) Then in chapter 5 we discuss cluster radioactivity in oganesson-294, the heaviest element ever produced by humans. In chapter 6 we move to the neutron-rich side of the nuclear chart ($N/Z > 1.8$ for 290Fm but not $^{254}_{98}\mathrm{Cf}_{156}$) to study isotopes which are expected to play a major role in the astrophysical r-process. **Along the way, we will discuss some of the issues related to fragment identification and yield prediction.**

Alternatively, at the end of each chapter, we say a few words about challenges faced during the project and new physical insights gained that aren't related to the overall narrative of the chapter, but which are nevertheless useful for future model developments.

Finally, in chapter 7 we discuss the current state of the field, and, based on our experience,

offer insights for guiding future developments in the field.

Chapter 2

Describing Fission Using Nuclear Density Functional Theory

Today there are 2 microscopic approaches to spontaneous fission that are in common use: time-dependent and static (time-independent). Time-dependent approaches evolve the system in real-time. Since fission is an inherently time-dependent process, these methods offer great insight into the fission process and the characteristics of the fragments, especially kinetic and excitation energies [13–17]. However, they can only treat a single event at a time and are quite expensive, making them impractical for fission yield predictions. Despite efforts such as [18, 19], there is currently no way to obtain a full yield distribution in a time-dependent framework. Furthermore, time-dependent computations tend to break down after too many time steps, making them unsuitable for tunneling. This is a problem because spontaneous fission is fundamentally a quantum mechanical tunneling process.

On the other hand, static approaches assume that collective motions of the nucleus are slow compared to the motion of the intrinsic particles, and therefore that collective and intrinsic degrees of freedom can be decoupled. This assumption, called the adiabatic approximation, justifies the creation of a potential energy surface (PES) in some space of collective shape coordinates. The dynamics of fission are then described as trajectories across the PES. Calculating the kinetic and excitation energies in this framework is straightforward

in principle, but in practice it is extremely sensitive to the scission configurations used. However, the static approach is much better suited to estimating fission yields and half-lives.

As we are trying to be as self-consistent as possible, we compute the PES in the framework of nuclear density functional theory, which combines the Hartree-Fock-Bogoliubov (HFB) mean-field approximation to the energy with a many-body method inspired by Kohn-Sham density functional theory (DFT). An overview of the self-consistent framework is described below, followed by the dynamical calculations which we use to calculate fission properties.

2.1 Nuclear Density Functional Theory

Since nuclei are quantum mechanical systems, they can in principle be described using the Schrodinger equation. However, in practice one finds this type of description difficult or impossible, for two reasons:

- In order to use the Schrodinger equation, one needs to know how to describe the interaction between particles, such as between protons and neutrons. However, protons and neutrons are made up of quarks and gluons, which interact via the strong nuclear force. Consequently, an analytic expression for the nucleon-nucleon interaction analogous to the $\frac{1}{r}$ form of the Coulomb interaction is not available. Finding different mathematical expressions which can describe the interaction between nucleons continues to be an active area of research [**?**]

- Even when an interaction is known, nuclei are large systems made up of many protons and neutrons. Solving the Schrodinger equation directly quickly becomes computationally intractable as the number of nucleons increases.

2.1.1 Density Functional Theory

Kohn-Sham DFT is based on the Hohenberg-Kohn theorems

Let us define the nucleon density in the following way: suppose we have a system described in second quantization by a set of creation and annihilation operators $c_i, c_i^\dagger$ which act on the [Fock-space?] vacuum state $|\psi_0\rangle$. The first Kohn-Sham theorem says that the energy of the system is a uniquely-defined functional of the density. That means that if a system of interacting particles and a system of noninteracting particles give the same density, the energy of those systems will be the same. This gives us the freedom to try to describe our system using a mean-field method instead of having to describe the pairwise interactions between every particle in the system - a huge simplification to the problem!

The second Kohn-Sham theorem states that the functional which gives the energy of the system will give the ground state energy if, and only if, it acts on the true ground state density. Thus, given a particular functional, we can vary the input density to minimize the total energy and be assured that we are approaching the ground state energy of the system.

Suppose you have the density $\rho(\mathbf{r})$ of an interacting system of particles. There exists a unique noninteracting system with the same density Then I believe HFB is put on top of that to do the variation part. I think I (approximately) get it now! - So just to make sure, what would DFT look like without HF/HFB? And HF/HFB without DFT?

Rather than find the density of a system of interacting particles (which can be extremely complicated - as one particle moves, the force it exerts on neighboring particles causes them to move, which will in turn change the magnitude and direction of the net force acting on the original particle, and so on until an equilibrium configuration, if it exists, can be attained), Kohn-Sham allows us to find an equivalent density of fictional non-interacting

particles. That is, instead of particles moving in a field generated by many interdependent neighboring particles, one may think of non-interacting particles moving about a mean-field, which is essentially an averaging over all other particles.

Together, the Hohenberg-Kohn theorems state that if one is able to find the true ground state density, regardless of where it comes from, then there exists a unique functional of the density which gives the ground state energy of the system. However, HK do not specify how this functional is to be obtained.

For a variety of reasons/complications (refs 73-78 of [5]), pure Kohn-Sham is not used in nuclear physics; however; in the spirit, we oftentimes switch to a representation involving densities (which are directly and exactly attainable from a many-body wavefunction) and energy density functionals (which are not known exactly). (Wait, but then what is the point of converting to densities? Why not just leave them as wavefunctions? Or maybe we do, but this representation just makes the math look nicer for papers)

The basic idea is to replace the single particle states $c_i^\dagger |\psi_0\rangle$ with the single-particle density, $\rho_{ij} = \langle\psi_0|c_j^\dagger c_i|\psi_0\rangle$

Because pairing interactions are of great importance to nuclear dynamics, we also construct an additional density $\kappa_{ij} = \langle\psi_0|c_j c_i|\psi_0\rangle$, which can be thought of as a coupling between the vacuum state and a state with two particles (in states i and j). Together with the single-particle density ρ we construct a generalized density

$$\mathcal{R} = \begin{pmatrix} \rho & \kappa \\ -\kappa^* & 1-\rho^* \end{pmatrix} \tag{2.1}$$

In coordinate space, the density matrix ρ and the pair tensor κ take the form

$$\rho(\vec{r},\vec{r}') = \langle\psi_0|c^\dagger_{\vec{r}'}c_{\vec{r}}|\psi_0\rangle \tag{2.2}$$

$$\kappa(\vec{r},\vec{r}') = \langle\psi_0|c_{\vec{r}'}c_{\vec{r}}|\psi_0\rangle \tag{2.3}$$

Recall that in nuclei, there is a ρ_n describing neutrons and a ρ_p for protons.

The total energy is a sum of several contributions:

$$E(\rho,\kappa) = E_{kin} + E_{Coul} + E_{nuc} + E_{pair} \tag{2.4}$$

where E_{kin} is the kinetic energy term, E_{Coul} contains the Coulomb interaction between protons, E_{nuc} is a phenomenological nucleon-nucleon interaction term, and E_{pair} describes the tendency of nucleons to form pairs, which is smeared out in non-interacting mean-field models. Finding a good nucleon-nucleon interaction E_{nuc} (and to a lesser extent, E_{pair}) to be used in calculations is an active topic of research in nuclear theory today (for one recent example, see [20]); two types of interactions which are commonly-used today are the Skyrme and Gogny families of interactions `\cite{???}`. We use primarily Skyrme-type interactions, which are described below.

2.1.1.1 Kinetic term

Defining the kinetic density $\tau_\alpha = \nabla\cdot\nabla'\rho_\alpha(\vec{r},\vec{r}')\big|_{\vec{r}=\vec{r}'}$, the kinetic energy contribution is

$$E_{kin} = \frac{\hbar^2}{2m}\left(1-\frac{1}{A}\right)\int d^3\vec{r}\left(\tau_n(\vec{r})+\tau_p(\vec{r})\right) \tag{2.5}$$

The $\left(1-\frac{1}{A}\right)$ term is a simple, approximate center-of-mass correction.

2.1.1.2 Coulomb interaction

The Coulomb interaction between protons is divided into a direct term and an exchange term, which is related to the Pauli exclusion principle.

$$E_{Coul} = E_{Coul,dir} + E_{Coul,exch} \tag{2.6}$$

$$E_{Coul,dir} = \frac{e^2}{2} \int d^3\vec{r}_1 d^3\vec{r}_2 \frac{\rho_p(\vec{r}_1)\rho_p(\vec{r}_2)}{|\vec{r}_1 - \vec{r}_2|} \tag{2.7}$$

$$E_{Coul,exch} = \frac{e^2}{2} \int d^3\vec{r}_1 d^3\vec{r}_2 \frac{\rho_p(\vec{r}_2,\vec{r}_1)\rho_p(\vec{r}_1,\vec{r}_2)}{|\vec{r}_1 - \vec{r}_2|} \tag{2.8}$$

Often the exchange term is computed in the Slater approximation \cite{refs 27,28 of HFODD-I}:

$$E_{Coul,exch} \approx -\frac{3e^2}{4}\left(\frac{3}{\pi}\right)^{\frac{1}{3}} \int d^3\vec{r}\rho_p^{\frac{4}{3}}(\vec{r}) \tag{2.9}$$

2.1.1.3 Skyrme interaction

The total Skyrme interaction energy density is a sum of both time-even and time-odd terms:

$$E_{Skyrme} = \int d^3\vec{r} \sum_{t=0,1} \left(\mathcal{H}_t^{even} + \mathcal{H}_t^{odd}\right) \tag{2.10}$$

$$\mathcal{H}_t^{even} = C_t^{\rho}\rho_t^2 + C_t^{\Delta\rho}\rho_t\Delta\rho_t + C_t^{\tau}\rho_t\tau_t + C_t^{J}\mathsf{J}_t^2 + C_t^{\nabla J}\rho_t\nabla\cdot\vec{J}_t \tag{2.11}$$

$$\mathcal{H}_t^{odd} = C_t^{s}\vec{s}_t^2 + C_t^{\Delta s}\vec{s}_t\Delta\vec{s}_t + C_t^{T}\vec{s}_t\cdot\vec{T}_t + C_t^{j}\vec{\mathsf{j}}_t^2 + C_t^{\nabla j}\vec{s}_t\cdot(\nabla\times\vec{j}_t) \tag{2.12}$$

where τ_t is the kinetic energy density; J_t is the spin current density, with vector part given by $\vec{J}_{\kappa,t} = \sum_{\mu\nu}\epsilon_{\mu\nu\kappa}\mathsf{J}_{\mu\nu,t}$; $\vec{s}_t$ is the spin density, $\vec{T}_t$ is the spin kinetic density; and $\vec{j}_t$ is the

momentum density (to see how these are related to ρ, see, e.g., [21]). The index $t = 0(1)$ refers to isoscalar(isovector) energy densities, e.g., $\rho_0 = \rho_n + \rho_p$ ($\rho_1 = \rho_n - \rho_p$). Note that $\mathcal{H}_t^{even}$ depends only on time-even densities (and likewise for $\mathcal{H}_t^{odd}$).

Since this interaction is phenomenological, based on a zero-range contact interaction between nucleons, the coefficients are adjustable. There are dozens of Skyrme parameterizations on the market, each one optimized to a particular observable or set of observables. The parameter sets SkM* [22] and UNEDF1 [23] (along with its sister, UNEDF1$_{\text{HFB}}$ [24]) are optimized to datasets which include deformed nuclei, making them suitable for fission.

2.1.1.4 Pairing interaction

We use a density-dependent pairing interaction:

$$E_{pair} = V_0 \int d^3\vec{r} \left(1 - \left(\frac{\rho(\vec{r})}{\rho_0}\right)^{\alpha}\right) \tag{2.13}$$

As with the nuclear interaction term, the pairing interaction contains several adjustable parameters.

2.1.2 Bogoliubov transformation

In anticipation of the HFB formalism below, we define the so-called Bogoliubov transformation. The fundamental entity in the Bogoliubov transformed basis are 'quasiparticle' states, defined by quasiparticle creation and annihilation operators acting on a quasiparticle vacuum state $|\Phi_0\rangle$ (in contrast to the single particle operators from before). The creation and annihilation operators are given by

$$\beta_\mu = \sum_i U^*_{i\mu} c_i + \sum_i V^*_{i\mu} c^\dagger_i \tag{2.14}$$

$$\beta^\dagger_\mu = \sum_i U_{i\mu} c^\dagger_i + \sum_i V_{i\mu} c_i \tag{2.15}$$

or in block matrix notation,

$$\begin{pmatrix} \beta \\ \beta^\dagger \end{pmatrix} = \begin{pmatrix} U^\dagger & V^\dagger \\ V^T & U^T \end{pmatrix} \begin{pmatrix} c \\ c^\dagger \end{pmatrix} \equiv \mathcal{W}^\dagger \begin{pmatrix} c \\ c^\dagger \end{pmatrix} \tag{2.16}$$

where the transformation matrix $\mathcal{W}$ must be unitary to ensure that $\beta, \beta^\dagger$ obey the fermion commutation relations [25]. In this transformed basis, the density matrix takes the form

$$\mathsf{R} = \mathcal{W}^\dagger \mathcal{R} \mathcal{W} = \begin{pmatrix} \langle\Phi_0|\beta^\dagger_\mu \beta_\nu|\Phi_0\rangle & \langle\Phi_0|\beta_\mu \beta_\nu|\Phi_0\rangle \\ \langle\Phi_0|\beta^\dagger_\mu \beta^\dagger_\nu|\Phi_0\rangle & \langle\Phi_0|\beta_\mu \beta^\dagger_\nu|\Phi_0\rangle \end{pmatrix} = \begin{pmatrix} 0 & 0 \\ 0 & I_N \end{pmatrix} \tag{2.17}$$

2.1.3 Hartree-Fock-Bogoliubov Equations

The ground state configuration of the system described by this particular energy density functional E is described by the density which minimizes $E(\mathcal{R})$. We can find this solution through the variational principle. We minimize the energy with respect to the generalized density, subject to the constraint that $\mathcal{R}^2 = \mathcal{R}$, or in other words, that the state remains a quasiparticle vacuum. Defining the HFB Hamiltonian $\mathcal{H}_{ba} \equiv 2\partial E/\partial \mathcal{R}_{ab}$, this variation leads to the result $[\mathcal{H}, \mathcal{R}] = 0$, which is called the Hartree-Fock-Bogoliubov equation. It is not typically solved in this form, but it can be recast into something more useful. Recalling that two Hermitian operators whose commutator is zero can be simultaneously diagonalized,

we choose to diagonalize $\mathcal{H}$ using the same Bogoliubov transformation W which diagonalizes $\mathcal{R}$:

$$W^{\dagger}\mathcal{H}W \equiv \mathcal{E} \qquad \text{or} \qquad \mathcal{H}W = W\mathcal{E} \tag{2.18}$$

where

$$\mathcal{E} = \begin{pmatrix} E_{\mu} & 0 \\ 0 & -E_{\mu} \end{pmatrix} \tag{2.19}$$

is a matrix of quasiparticle energies. In this form, the problem can then be solved iteratively: an initial density ansatz is chosen in order to construct the Hamiltonian density $\mathcal{H}$, after which the eigenvalue problem is solved, leading to new densities (since the densities are related to $\mathcal{W}$), which in turn leads to an updated $\mathcal{H}$. This procedure can be repeated indefinitely, until some predetermined convergence criterion is met.

Very often we will want to minimize the energy with the system subject to a particular constraint. In that case we would replace the Hamiltonian E with the Routhian E' before variation. Typically E' introduces the constraints via the method of Lagrange multipliers. Some common examples might be this simple form of particle number restoration (more sophisticated forms, such as Lipkin-Nogami `\cite{???}`, also exist)

$$E' = E - \lambda_n \left\langle \hat{N}_n \right\rangle - \lambda_p \left\langle \hat{N}_p \right\rangle \tag{2.20}$$

where λ_{α} is determined later by the condition that $\left\langle \hat{N}_{\alpha} \right\rangle = N_{\alpha}$, or shape, where we might constrain a particular multipole moment (or set of multipole moments) to the value $\bar{Q}_{\lambda\mu}$

$$E' = E - \sum_{\lambda\mu} C_{\lambda\mu} \left(\left\langle \hat{Q}_{\lambda\mu} \right\rangle - \bar{Q}_{\lambda\mu} \right)^2 \tag{2.21}$$

2.1.4 Nucleon localization function

One of the tools we will be using quite a bit in this thesis is the nucleon localization function (NLF), introduced in [26]. The NLF is defined using the single particle density in the following way (with q=isospin and σ=spin/signature quantum number):

$$\mathcal{C}_{q\sigma} = \left[1 + \left(\frac{\tau_{q\sigma}\rho_{q\sigma} - \frac{1}{4}|\nabla\rho_{q\sigma}|^2 - \mathbf{j}_{q\sigma}^2}{\rho_{q\sigma}\tau_{q\sigma}^{TF}} \right)^2 \right] \tag{2.22}$$

where $\tau_{q\sigma}^{TF} = \frac{3}{5}(6\pi^2)^{\frac{2}{3}}\rho_{q\sigma}^{\frac{5}{3}}$. A localization value $\mathcal{C} \approx 1$ means that nucleons are well-localized; that is, the probability of finding two nucleons of equal spin and isospin at the same location in space is low. A value of $\mathcal{C} = \frac{1}{2}$ corresponds to a Fermi gas of nucleons, as found in nuclear matter.

The NLF offers greater insight into the underlying shell structure of the system than, for instance, the single particle density. In particular, when applied to fission as in [27], it sometimes enables one to see the formation of well-defined prefragments whose shell structure is responsible for the peak of the fragment distribution. A method for identifying fission fragments and estimating fragment distributions using the NLF is described in Appendix A.

2.2 Microscopic Description of Nuclear Fission

With the nuclear physics somewhat under control, we now move onto the problem of using it to describe fission. Recently in [28], an approach based on this assumption was used

to compute fragment yields from a potential energy surface (PES) that was computed self-consistently, using the WKB approximation to describe the tunneling and Langevin dynamics to describe post-scission dissipation. The half-life can be computed as in [29].

2.2.1 Potential Energy Surfaces

In the adiabatic approximation, the primary degrees of freedom are nuclear shapes, and therefore the basic ingredient to fission calculations is a potential energy surface (PES). In principle, one could describe any three-dimensional shape using an infinite basis such as the multipole expansion which is often encountered in electrodynamics; however, for practical computations one must used a truncated set of only a few collective coordinates. Thus, an important challenge for researchers is to select the most relevant collective coordinates, ideally while demonstrating that others can be safely neglected. Often one will use the first few lowest-order multipole moments; however, multipole moments may not always be well-suited to describing shapes which occur during fission, especially near scission. One alternative was proposed in [30].

Once the appropriate shape constraints are chosen, the PES is computed as a mesh: one DFT calculation per grid point. The value at each point is the HFB energy computed above, $E'(\vec{q})$.

2.2.2 Collective inertia

Just as important to the fission dynamics as the energy of the system is the collective inertia, which describes the tendency of the system to resist configuration changes (such as shape changes). The form of the collective inertia we use is the non-perturbative adiabatic time-

dependent HFB (ATDHFB) inertia with cranking [31], which takes the form

$$\mathsf{M}_{\mu\nu} = \frac{\hbar^2}{2}\frac{1}{(E_a + E_b)}\left(\frac{\partial \mathcal{R}^{21}_{(0),ab}}{\partial q_\mu}\frac{\partial \mathcal{R}^{12}_{(0),ba}}{\partial q_\nu} + \frac{\partial \mathcal{R}^{12}_{(0),ab}}{\partial q_\mu}\frac{\partial \mathcal{R}^{21}_{(0),ba}}{\partial q_\mu}\right) \tag{2.23}$$

The subscripts and superscripts are explained in the full temperature-dependent derivation of the collective inertia found in Appendix B, but the important feature to note is that computing the inertia requires differentiating the density matrix with respect to a set of collective coordinates.

A perturbative expression for the ATDHFB inertia also exists, which allows one to estimate the inertia without taking derivatives of the density. It is computationally much faster and easier to implement, but it is less accurate and loses many of the important features of the inertia, as we shall see in Chapter 5. Nevertheless, it is commonly-used in calculations and we shall use it later on.

Another common expression for the collective inertia comes from the Generator Coordinate Method (GCM). The GCM inertia also exists in two varieties: perturbative and non-perturbative [32]. Like the ATDHFB inertia, the perturbative GCM inertia is smoothed-out compared to the non-perturbative inertia. Both the perturbative and non-perturbative GCM inertias are found to be smaller in magnitude than their ATDHFB counterparts.

2.2.3 WKB Approximation

Spontaneous nuclear fission is a type of quantum tunneling; consequently, it should be described using quantum mechanics. If the wavefunction corresponding to the fissioning nucleus is assumed to be slowly-varying inside the potential barrier (which is the case under the adiabatic assumption), then the WKB approximation allows us to estimate the tunneling

probability through a classically-forbidden region in the PES.

Consider a set of collective coordinates $\mathbf{q} \equiv (q_1, \ldots, q_N)$. The most-probable tunneling path $L(s)|_{s_{\text{in}}}^{s_{\text{out}}}$ in the collective space is found via minimization of the collective action

$$S(L) = \frac{1}{\hbar} \int_{s_{\text{in}}}^{s_{\text{out}}} \sqrt{2\mathcal{M}(s)\,(V(s) - E_0)} ds, \tag{2.24}$$

where s is the curvilinear coordinate along the path L, $\mathcal{M}(s)$ is the collective inertia given by [29]

$$\mathcal{M}(s) = \sum_{\mu\nu} \mathsf{M}_{\mu\nu} \frac{dq_\mu}{ds} \frac{dq_\nu}{ds} \tag{2.25}$$

and $V(s)$ is the potential energy along $L(s)$. E_0 stands for the collective ground-state energy. The dynamic programming method [33] is employed to determine the path $L(s)$. The calculation is repeated for different outer turning points, and each of these points is then assigned an exit probability $P(s_{\text{out}}) = [1 + \exp\{(2s)\}]^{-1}$ [34].

The half-life corresponds to the minimum action pathway, and the expression for the half-life is $T_{1/2} = \ln(2)/nP(s_{\text{min}})$. The parameter n is the number of assaults on the fission barrier per unit time and the standard value is $n = 10^{20.38} s^{-1}$.

2.2.4 Langevin Dynamics

Two techniques for predicting fission fragment yields are the Langevin approach used by [28] and the Time-Dependent Generator Coordinate Method (TDGCM) approach used in [30]. I will be using Langevin dynamics, which are described in this section.

After emerging from the classically-forbidden region of the PES, fission trajectories begin from the outer turning line and then evolve along the PES according to the Langevin

equations:

$$\frac{dp_i}{dt} = -\frac{p_j p_k}{2}\frac{\partial}{\partial q_i}\left(\mathcal{M}^{-1}\right)_{jk} - \frac{\partial V}{\partial q_i} - \eta_{ij}\left(\mathcal{M}^{-1}\right)_{jk} p_k + g_{ij}\Gamma_j(t)\,, \tag{2.26}$$

$$\frac{dq_i}{dt} = \left(\mathcal{M}^{-1}\right)_{ij} p_j\,, \tag{2.27}$$

where p_i is the collective momentum conjugate to q_i. The dissipation tensor η_{ij} is related to the random force strength g_{ij} via the fluctuation-dissipation theorem, and $\Gamma_j(t)$ is a Gaussian-distributed, time-dependent stochastic variable.

The fluctuation-dissipation theorem is given by the expression $\sum_k g_{ik}g_{jk} = \eta_{ij}k_B T$. It effectively couples the collective and intrinsic via the system temperature, given by $k_B T = \sqrt{E^*/a}$ where $a = A/10\text{MeV}^{-1}$ parameterizes the level density and the excitation energy $E^* = V(s_{out}) - V(\mathbf{x}) - \frac{1}{2}\sum\left(\mathcal{M}^{-1}\right)_{ij} p_i p_j$.

Dissipation is treated in our work as a parameter, as a self-consistent description of dissipation is not yet known. However, work along this line has been started (maybe?) in refs 291-293 of [35] (see section 4.1.1 for the context). In the meantime, we use the values from [28] (Is this too specific for a thesis? You're not worried about the little numerical details, right? Just the big-picture ideas?)

Chapter 3

Numerical implementation

Since this modern era of fission theory takes advantage of high-performance computers, it is worth taking some time to discuss some of the issues which came up during the course of this research, and how modern computing tools were used to solve the problem.

3.1 Calculating the PES

By far, the most time-intensive part of a microscopic fission calculation is the calculation of the PES. For this we use a pair of DFT solvers, HFODD [36] and HFBTHO [37]. These programs solve the HFB equations in a basis of deformed harmonic oscillators. The solver HFBTHO is limited to shapes with axial symmetry, while HFODD allows for the breaking of any symmetry needed. Broken symmetries mean that each matrix element must be computed independently, while good symmetries mean However, since the major bottleneck of each of these programs involves constructing matrices representing Skyrme densities and currents and then diagonalizing the matrix representing the HFB Hamiltonian, this flexibility drastically increases the time-to-solution.

On the positive side, the problem of calculating a PES is embarrassingly-parallel. So while an individual point in the PES may be difficult to compute, many points can be computed simultaneously. This does have its limitations; highly-deformed configurations may be very unstable because of reasons. One fix may sometimes be to use a nearby point

which converged successfully as a seed function

The procedure is performed iteratively: First, an ansatz is given for the density (either by the user or by some simple means, such as a quick Woods-Saxon calculation). Then the energy density matrix is constructed, after which it is diagonalized and a new density matrix is calculated. The procedure then repeats for a fixed number of iterations, or until a predetermined convergence criterion is satisfied In HFODD, for instance, the default convergence criterion is for the difference between the total energy summed over all single-particle states and the total energy calculated by `???` to be less than some user-defined value.

Certain parts of the procedure can be parallelized using shared-memory parallelism, such as QMULCM, which does what again? It readjusts the Lagrange parameters of the constraints based on the perturbative approximation fot he QRPA matrix.

3.1.1 PES Tools

Apart from the issue of walltime, generating a PES creates a lot of output files, which quickly becomes unwieldy. To help manage all this data, a Python module called PES Tools was created for manipulating, extracting, interpolating, and plotting PES data [**?**]. Aside from solver-dependent parser scripts, which collect data from the output of a DFT run and store it in the XML file format, PES Tools is not dependent on a particular DFT solver.

In particular, a submodule was created to interface between PES Tools and Fission Tools [**?**], a set of codes which have relevance to fission calculations. Many of these codes are described in the following sections.

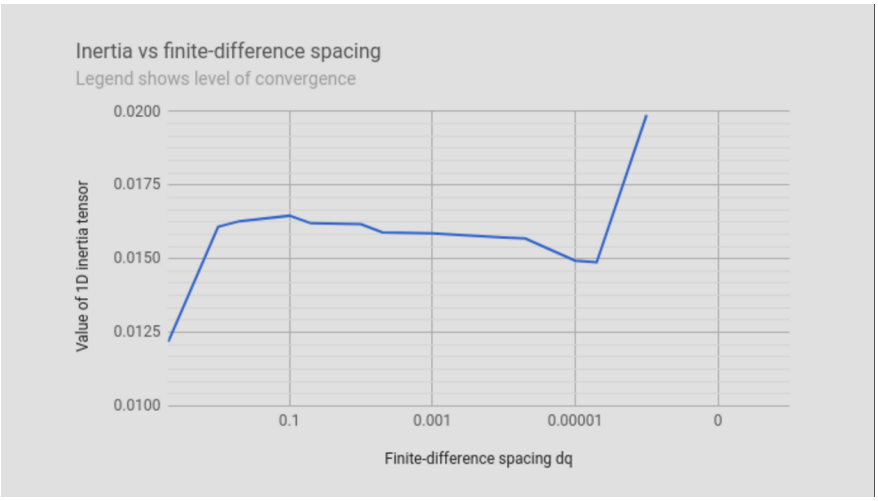

Figure 3.1: $\mathcal{M}_{22}$ calculated for ??? configuration of ^{240}Pu as a function of finite-difference spacing.

3.2 Calculating the collective inertia

The partial derivatives from equation 2.23 are computed using the Lagrange three-point formula:

$$\left(\frac{\partial \mathcal{R}}{\partial q}\right)_{q=q_0} \approx \frac{-\delta q'}{\delta q\,(\delta q + \delta q')}\mathcal{R}(q_0 - \delta q) + \frac{\delta q - \delta q'}{\delta q \delta q'}\mathcal{R}(q_0) + \frac{\delta q}{\delta q'\,(\delta q + \delta q')}\mathcal{R}(q_0 + \delta q') \quad (3.1)$$

The accuracy and precision of the collective inertia $\mathcal{M}$ are therefore functions of the spacings δq and $\delta q'$, and of $\mathcal{R}$. An accurate value of the collective inertia is especially important for computing half-lives, where there is an exponential dependence on $\mathcal{M}$.

Figure 3.1 shows the effect of different values of $\delta q = \delta q'$ on the collective inertia for a particular configuration of ^{240}Pu.

Figure 3.1 shows the norm of the matrix which corresponds to the difference between the density matrix at the last iteration and the second-to-last iteration. Predictably, the norm decreases as the convergence parameter becomes tighter. This gives a sense of the uncertainty

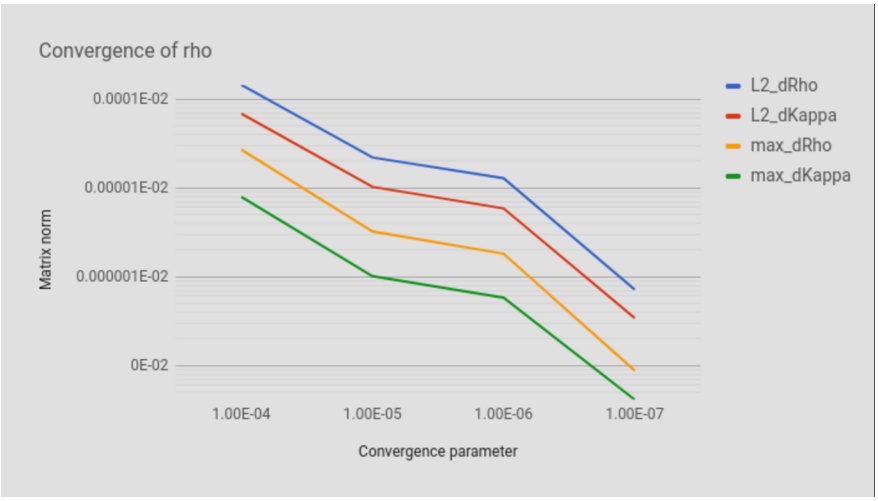

Figure 3.2: Norm of the difference matrix between subsequent iterations of the density.

associated with the density, which in turn should be propagated through equations 3.1 and 2.23.

There are additional complications which arise in the finite-temperature formalism. These are discussed in Appendix B.

3.3 Minimum action path

For the tunneling described in Section 2.2.3, the dynamic programming method [33] was used to minimize the action. The dynamic programming scheme proceeds inductively: Once the minimum action is known for all grid points up to a certain value of Q_{20}, say q_{20}^n, then the minimum action at each grid point in the layer with $Q_{20} = q_{20}^{n+1}$ is obtained by computing the action between each grid point in layer n and each grid point in layer $n+1$, and then finding the path which minimizes the total action at each grid point in layer $n+1$:

$$S_{min}(\vec{Q})\Big|_{Q_{20}=q_{20}^{n+1}} = \text{argmin}_{\vec{Q}'}\left(S_{min}(\vec{Q}') + \Delta S_{min}(\vec{Q},\vec{Q}')\right)\Big|_{Q'_{20}=q_{20}^{n},Q_{20}=q_{20}^{n+1}}. \quad (3.2)$$

The inductive step which connects layers n and $n+1$ involves several small, independent calculations which lend themselves well to shared-memory parallelism. This was implemented in the code using OpenMP, resulting in a walltime reduction from order $\mathcal{O}(n^D)$ to $\mathcal{O}(n^D/m)$, where m is the number of processors (with the usual caveats that parallelization requires some additional overhead time, and that the actual speedup might be somewhat less when the number of processors m reaches the same order as the number of points per layer n^{D-1}). In a 2D calculation, where the runtime is on the order of seconds, the difference is inconsequential. However, this speedup was essential for the analysis of a 4D PES, as described in Chapter 5.

3.4 Langevin

Once the action and relative probability are known for a set of points along the outer turning line, Langevin trajectories are computed originating from each outer turning point. These are straightforwardly evaluated at discrete time steps over a discretized PES mesh.

Because of the random force term in equation 2.26, a large number of trajectories per outer turning point must be computed to reduce statistical uncertainty. Fortunately, each trajectory is completely independent of every other trajectory, lending the code readily to shared-memory parallelism. However, for the Fission Tools Langevin code I chose to use distributed-memory parallelism instead of shared-memory parallelism in order to simplify access to shared resources, such as variables and output files.

Chapter 4

Two fission modes in ^{178}Pt

4.1 Asymmetric fission in the region of ^{180}Hg

As mentioned in the introduction, fission is most well-studied in the region of the actinides (Z=90 to Z=103), as many naturally-occurring isotopes in this region are fissile. Within this region, there is a characteristic tendency for fission fragment yields to be asymmetric (that is, one light fragment and one heavy fragment), with the heavy peak centered around $A \approx 140$. This has been understood as a manifestation of nuclear shell structure in the prefragments: doubly-magic ^{132}Sn drives the nucleus towards scission, and once the neck nucleons are divided up between the two fragments, we end up with the heavy fragment A=140 peak. As one moves to the lower-Z actinides, however, this tendency becomes less and less pronounced as yields tend to become more symmetric. Below thorium, it was generally believed until recently (though mostly not tested) that yields would continue to be symmetric as there was no doubly-magic nucleus candidate that could drive the system toward asymmetry as there is with actinides.

However, it was reported in a 2010 study [38] that neutron-deficient ^{180}Tl undergoes beta-delayed fission, leading to intermediate state $^{180}_{80}\mathrm{Hg}_{100}$ which then decays into two fragments of unequal mass. This finding triggered a flurry of theoretical papers hoping to describe this new and unexpected phenomenon (for instance, see `\cite{some papers}`). A follow-up

study using ^{178}Tl [39] further established this as a region of asymmetric fission, and not just a one-time occurrence. Since then, other nuclei in the region have been studied, for instance using Coulex-induced fission reactions and compound nucleus (prompt?) fusion-fission reactions, and the finding is the same.

Nuclei in this region have a number of unique features which make them interesting for study, even aside from the unexpected fragment asymmetry. Predicted fission barrier heights in this region are relatively-low (of the order of 12 MeV), making them suitable for study using low-energy techniques such as β-delayed fission (maybe [40] and the work at ISOLDE at CERN?) or Coulex-induced fission (maybe [41] and the SOFIA (Studies On FIssion with Aladin) experiment/project/campaign). On the other hand, it has been found that compound nuclei formed in this region from particle-induced reactions tend to have high excitation energies, even for beam energies near the Coulomb barrier. This combination makes the region particularly well-suited for studies involving a variety of excitation energies.

Later experiments performed with isotopes in this region at different excitation energies have shown that, unlike the case of actinides where shell structure and fragment asymmetry is "washed out" at high excitation energies, mass asymmetric fragment distributions are a persistent feature of this mass region for various excitation energies. (A lot of good citations for this section can come from section 4.1.1 of [42]) An up-to-date (as of around 2016) overview of nuclei in the region of $^{180}_{80}\mathrm{Hg}_{100}$ which have since been experimentally studied, including the experimental technique used, is shown in Figure 4.1.

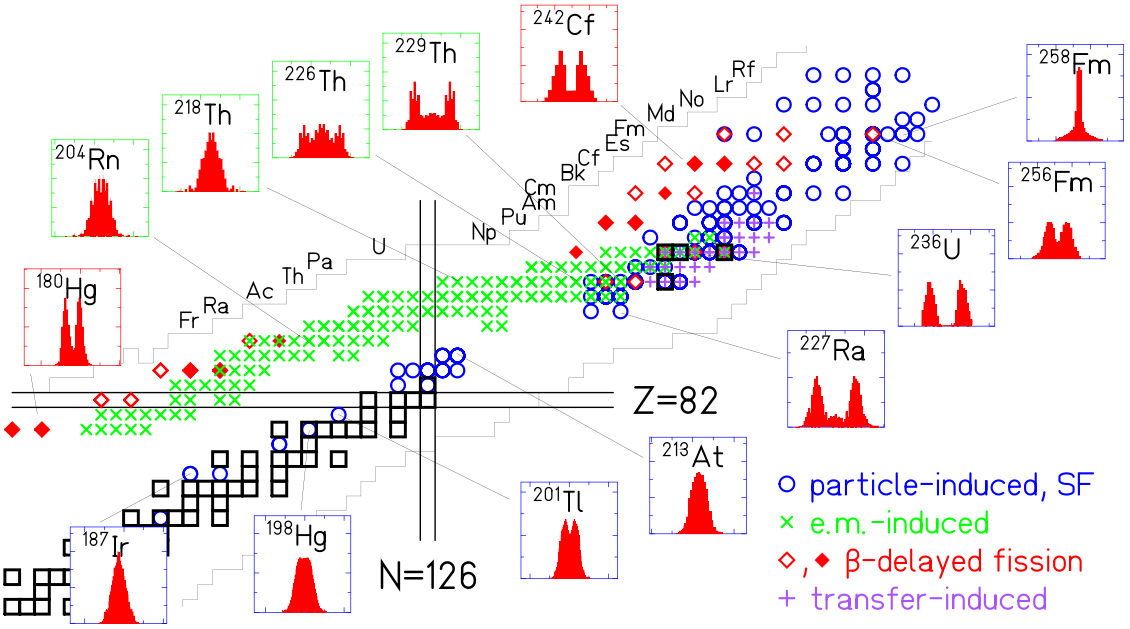

Figure 4.1: Fragment yields for several nuclei ranging from actinides, where primary fission yields tend to be asymmetric, down to near-thorium, where yields become more symmetric except in the region near neutron deficient $^{180}_{80}\mathrm{Hg}_{100}$. Figure from [42].

4.2 Multimode fission of ^{178}Pt

One particular follow-up experiment was performed investigating spontaneous fission of $^{178}_{78}\mathrm{Pt}_{100}$ [**?**], which differs from $^{180}_{80}\mathrm{Hg}_{100}$ by 2 protons. This system was studied at various excitation energies and found to fission consistently with a bimodal pattern, as shown in Figure 4.2. Of the nuclei which underwent spontaneous fission, roughly 1/3 were found to fission symmetrically while the other 2/3 fissioned asymmetrically with a light-to-heavy mass ratio of approximately 79/99. Furthermore, it was observed that symmetric fragments tended to have higher kinetic energies than non-symmetric fragments.

To better interpret the results of this experiment, DFT calculations were performed using the functionals $\mathrm{UNEDF1}_{\mathrm{HFB}}$ [24] and D1S [43]. These calculations involved computing a PES using the collective coordinates Q_{20} and Q_{30}. [Do I need to describe the calculations in detail here, or should I refer to the published papers (e.g. "Details of the calculation are

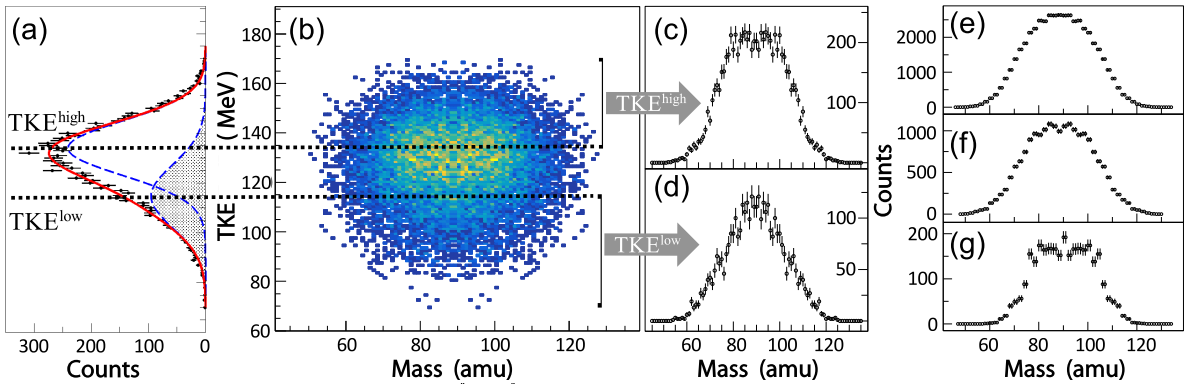

Figure 4.2: This figure contains the data from the $^{178}_{78}\mathrm{Pt}_{100}$ experiment. I should go through and describe what all the individual boxes are for. Then I should cite out paper, once it's citeable

given in `the paper`")?]

The UNEDF1$_{\mathrm{HFB}}$ PES is shown in Figure 4.3, while the D1S PES is in Figure 4.4. A calculation with full Langevin dynamics was not performed; however, the static (minimum-energy) pathway shown in the figure corresponds to a fragment split $A_L/A_H \approx 80/98$.

Also shown in Figure 4.3 are nucleon localization functions (recall Section) corresponding to various configurations in the PES. Along the symmetric path (ABcd in the figure), the fragments appear highly-elongated, with a rather large neck, even shortly before scission. Since elongation tends to minimize the Coulomb repulsion between fragments, then this configuration might be expected to lead to fragments with relatively low kinetic energies. On the other hand, compact fragments such as those in ABCD will tend to have a larger Coulomb repulsion, propelling the fragments away from one another with greater force and resulting in fragments with a higher kinetic energy. [We note that this is compatible with experiment]

Now consider the PES corresponding to the D1S functional in Figure 4.4. We note with some relief that, despite the inherent differences between the functionals, and despite the relative flatness of the surface with few discernible topological features, the overall topology

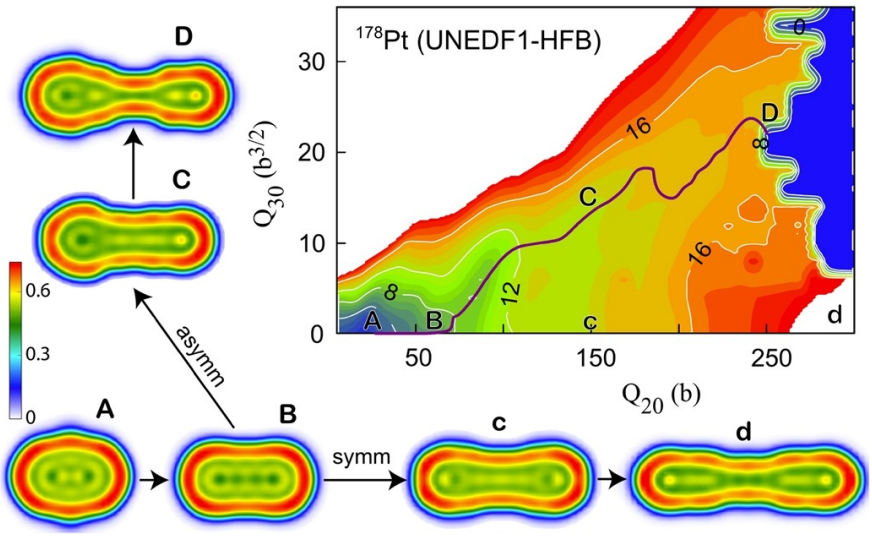

Figure 4.3: UNEDF1-HFB potential energy surface for ^{178}Pt. Note the two different trajectories ABCD and ABcd and their corresponding localizations.

of the PES is similar in both cases. The overall magnitude is different, but the static pathway follows a similar trajectory.

4.3 The physical origin of fragment asymmetry in the region of ^{180}Hg

Why is there a region of symmetric fission below thorium?

(These are notes from the 178Pt paper draft. Not mine, of course, but they have some good points to address): "Namely, the PES are predicetd to be flat and much less structureless, and defined predominantly by the large liquid drop/macroscopic contribution, rather than by relatively small microscopic effects. Due to this, FFMDs exhibit fairly low dependence.. [refer to 180Hg PLB, as one example].

"(this was an answer by Witek, when somebody asked a question to my talk at Tsukuba - why the lead region is less sensitive to temperature.. the answer was - there is no 'barrier'

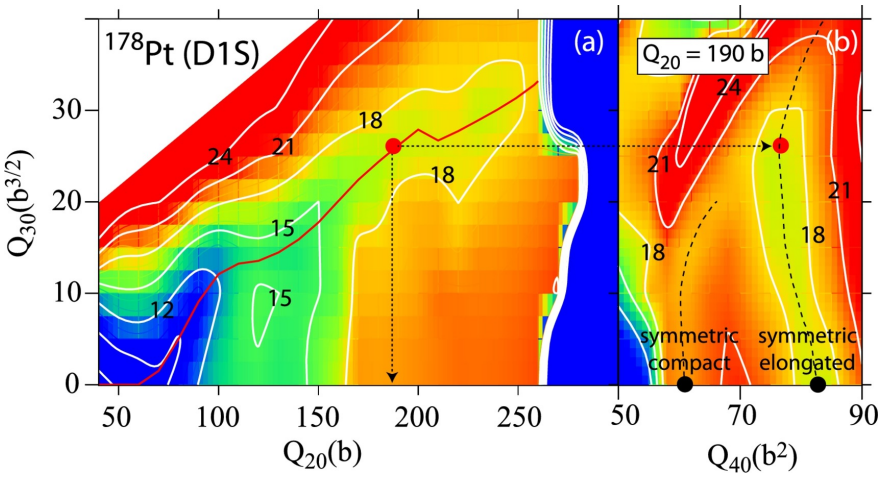

Figure 4.4: D1S potential energy surface for ^{178}Pt. Note also the additional information about the hexadecapole moment.

in a sence, it's just flat/thick macroscopic surface, hardly influenced by shell effects.. so, even if one heats it up, tiny shell effects will be gone, but the main underlying macroscopic part will remain)."

Peter Moller argues in the concluding discussion of (https://link.aps.org/doi/10.1103/PhysRevC.85.024 [44]) that we can't really use the fragment/prefragment shell structure arguments in this region, and thus that we have yet to identify all the essential physics which determines fragments. He says the yields are given (at least in this case) by subtle interplays in local regions of the potential energy surface.

Witek, Michal Warda, and Staszczak argue in Section IV. *Prescission Configurations* of [45] that 180Hg deforms as a molecular system consisting of 90Zr and 72Ge, with the remaining neck nucleons being distributed at scission to give the fragments they found in the experiment. Similarly, they make the same claim for 198Hg, except using 98Zr and 80Ge. The first one kind of makes sense to me since 90Zr is semi-magic, but 98Zr is not and neither is 80Ge. I wonder what might have happened had they tried to match up the densities of a different set of nearby nuclei (they used these because they had the same N/Z ratio as the

fissioning parent nucleus). Then in the conclusions: "We conclude that the mass distribution of fission fragments in both nuclei is governed by shell structure of prescission configurations associated with molecular structures."

In the introduction to [46] it is stated as though conclusively that "the main factor determining the mass split in fission are shell effects at pre-scission configurations, i.e., between saddle and scission" (see also some additional references therein). I think the thing that is most selling it to me so far, though, is Fig. 3 from this paper, wherein they show the shell correction energy for each of the nuclei considered. Even though the PES itself is mostly flat in each of these cases, the magnitude of the shell correction is different whether you are looking at symmetric or asymmetric trajectories, and the one with the larger magnitude shell correction happens to be the one that wins out in the final fragment distribution. I'd also be curious to see what the collective inertia looks like, but this seems to at least give something. It's not like this shell correction gets added on top of the PES - the PES is still relatively-flat - but it at least gives an explanation for why our traditional physical intuition is not totally failing us here.

Interesting future work in this region might include calculations with full dynamics (including from nuclei with excitation energy), as suggested in the conclusions of [46]

Chapter 5

Cluster decay in ^{294}Og

5.1 Cluster emission in Superheavy Elements

The region of superheavy elements (Z>104) is an interesting one for the study of spontaneous fission because the liquid drop model predicts that all isotopes with Z>104 are unstable with respect to spontaneous fission. These nuclei are stabilized due to shell effects, but they nevertheless remain short-lived and many of them will decay by spontaneous fission regardless.

Experimentally, spontaneous fission has been observed from several superheavy isotopes (see the right panel of Figure 5.1). Other observed SHEs undergo a series of alpha decays, which chains terminate in spontaneous fission. Furthermore, a variety of models predict regions of spontaneous fission in the superheavy regime. One example is shown in Figure 5.1, in which lifetimes were computed for several types of decays using empirical formulas and the results compared to estimate branching ratios. Figure 5.2 is similar, except that the spontaneous fission lifetimes were computed microscopically, as were the Q_α values used to estimate alpha decay lifetimes.

cluster emission [49–51]

From the theoretical point of view, half-life calculations based on semiempirical models predict cluster radioactivity to be the dominant decay channel of several superheavy nu-

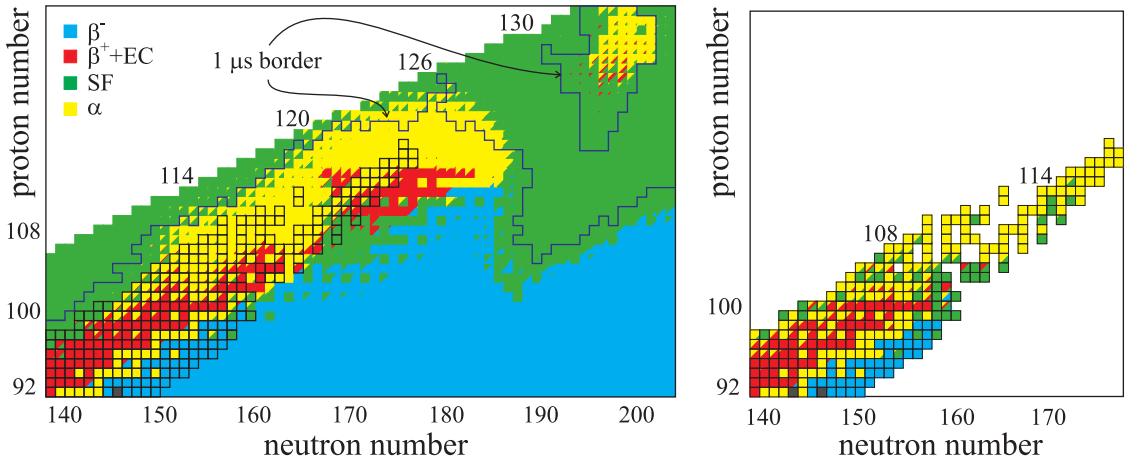

Figure 5.1: Calculated (left) and experimental (right) decay modes for SHE, based on an analysis of lifetimes calculated via empirical formulae. The boxed isotopes in the left panel are those which have been measured experimentally. Isotopes falling inside the 1μs contour are predicted to live longer than 1μs. Figure adapted from [47].

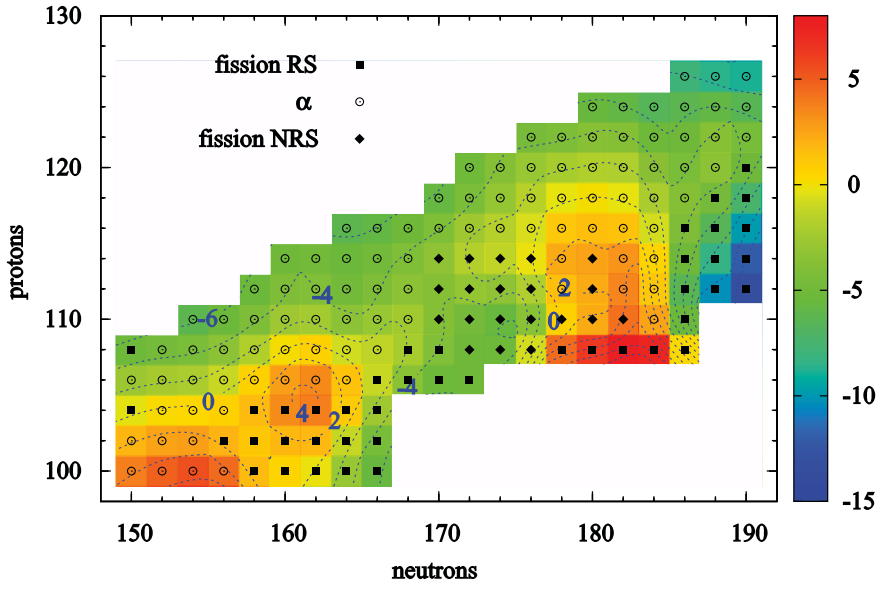

Figure 5.2: Dominant decay modes for SHE in a nuclear DFT-based framework are indicated. The label "RS" stands for "reflection symmetric" and "NRS" stands for "non-reflection symmetric." The colorbar indicates the predicted half-life on a logarithmic scale. Figure from [48].

clei [52–58]. Similar predictions have been obtained by more microscopic calculations using nuclear DFT framework [59, 60].

Poenaru and others have predicted in [52–58] that many superheavy elements will decay into two fragments, with the heavy fragment near the doubly-magic nucleus $^{208}_{82}\mathrm{Pb}_{126}$. This particular decay mode is significant enough to have earned its own name in the literature, where it is known variously as cluster emission, cluster radioactivity, or lead radioactivity [49–51, 61]. The phenomenon of cluster emission was first observed in the decay $^{223}_{88}\mathrm{Ra}\rightarrow^{209}_{82}\mathrm{Pb} + ^{14}_{6}$ [62] and has since been observed in several actinides. In all cases seen so far, it is a rare event with a small branching ratio [61].

The mechanism of cluster emission is based on the stability of the doubly-magic nucleus $^{208}_{82}\mathrm{Pb}_{126}$. $^{294}_{118}\mathrm{Og}_{176}$ is an excellent candidate for cluster emission because the cluster it is predicted to emit, $^{86}_{36}\mathrm{Kr}_{50}$, receives additional stability due to its having a magic number of neutrons. Semiemprical arguments based on the symmetry energy lend additional support to this candidate, since $^{294}_{118}\mathrm{Og}_{176}$ and $^{208}_{82}\mathrm{Pb}_{126}$ have a similar N/Z ratio [60].

We took this prediction one step further than the aforementioned by calculating the full spontaneous fission fragment distribution of $^{294}_{118}\mathrm{Og}_{176}$. As we will show, the distribution is sharply-peaked around $^{208}_{82}\mathrm{Pb}_{126}$. Furthermore, the distribution is quite robust with respect to the inputs of the calculations. We will also visualize the formation of the fragments using the nucleon localization function.

5.2 Predicted spontaneous fission yields of ^{294}Og

We calculated the spontaneous fission fragment yields for $^{294}_{118}\mathrm{Og}_{176}$ under a variety of conditions. First, we elected to using three distinct EDFs: UNEDF1$_{\mathrm{HFB}}$[24], a Skyrme functional

which was optimized to data for spherical and deformed nuclei, including fission isomers; SkM* [22], another Skyrme functional designed for fission barriers and surface energy; and D1S [43], a parameterization of the finite-range Gogny interaction fitted on fission barriers of actinides.

A different collective space was used with each EDF for the tunneling portion of the PES. The UNEDF1$_{\mathrm{HFB}}$ calculation was carried out in a four-dimensional collective space consisting of the collective coordinates $(Q_{20}, Q_{30}, Q_{22}, \lambda_2)$. By examining this PES, we were able to reduce to dimensionality of the PES for the other two functionals. The SkM* calculation was performed in a piecewise-continuous space. Between the ground state and the isomer state, Q_{30} does not play a significant role and so the system was described using $(Q_{20}, Q_{22}, \lambda_2)$. Likewise, $Q_{22} \approx 0$ once the isomer state is reached and reflection symmetry is broken ($Q_{30} \neq 0$), suggesting use of the coordinates $(Q_{20}, Q_{30}, \lambda_2)$. Finally, for the functional D1S we decided to see how our yields would be affected if we did not consider dynamical pairing fluctuations or axial symmetry breaking at all, in order to drastically reduce computation time. Those calculations were performed in the collective space (Q_{20}, Q_{30}).

In the region of Langevin dynamics, which is the region connecting the hypersurface of outer turning points and to the hypersurface of scission points, we found again that $Q_{22} \approx 0$. Consequently, this region was limited to two dimensions (Q_{20}, Q_{30}) in all cases.

We start by showing 2-dimensional projections of the calculated PESs in Figure 5.3. Although the collective spaces used are different, it is reassuring to see that the surfaces strongly resemble one another. Some common features we highlight are: a symmetric saddle point occurring around $Q_{20} \approx 40\,\mathrm{b}$; a second barrier beginning around $Q_{20} \approx 100 - 120\,\mathrm{b}$ along the symmetric fission path; the presence of local minima at large deformations (marked by stars in the figure); a deep valley that leads to an highly-asymmetric split; and the

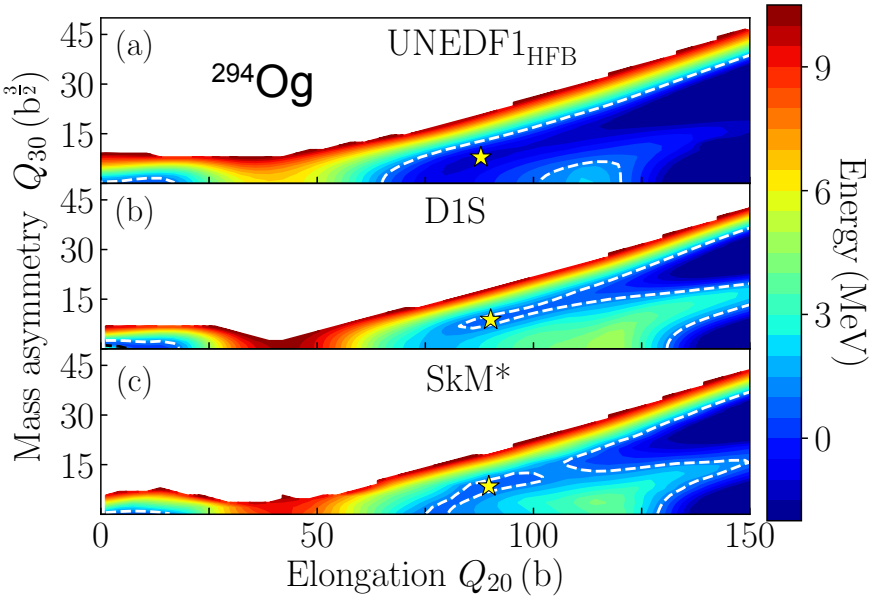

Figure 5.3: Comparison of the PESs for $^{294}_{118}\mathrm{Og}_{176}$ in the (Q_{20}, Q_{30}) collective plane obtained in UNEDF1$_{\mathrm{HFB}}$ (a), D1S (b), and SkM* (c) EDFs. The ground-state energy E_{gs} is normalized to zero. The dotted line in each figure corresponds to $E_0 - E_{gs} = 1\,\mathrm{MeV}$, which was used to determine the inner and outer turning points. The local energy minima at large deformations are marked by stars.

secondary, less-asymmetric fission valley that emerges at large elongations.

But there are differences as well, such as the height of the first saddle point, the depth of the highly-asymmetric fission valley, and the height of the ridge separating the two fission valleys. As a result, the outer turning points are pushed to larger elongations in D1S and SkM* as compared to UNEDF1$_{\mathrm{HFB}}$. These differences in the PES topology strongly affect the predicted spontaneous fission half-lives τ_{SF}, which in the case of UNEDF1$_{\mathrm{HFB}}$, SkM* and D1S are $9.1 \times 10^{-9}\,\mathrm{s}$, $4.0 \times 10^{-5}\,\mathrm{s}$ and $3.2 \times 10^{-2}\,\mathrm{s}$, respectively (see also [63, 64] for a detailed discussion of half-lives). These large variations of τ_{SF} reflect the well-known exponential sensitivity of spontaneous fission half-lives to changes in the quantities entering the collective action (2.24). The τ_{SF} predictions of UNEDF1$_{\mathrm{HFB}}$ and, to a lesser degree, SkM* are incompatible with experiment, as ^{294}Og is known to decay by α-decay with a half-life of 0.58 ms [65]. This observation could in fact also apply to the D1S results, since the

D1S calculations were performed in a smaller collective space leading to overestimation of the half-lives [66, 67]. It is to be noted that while half-lives are very sensitive to details of the calculations, the models used here are very consistent with each other and with experiment when it comes to global observables, such as alpha-decay energies, deformations, and radii [68, 69]. As demonstrated below in Figure 5.4, spontaneous-fission mass and charge yields are also robustly predicted.

As expected, the yields are peaked in the region of ${}^{208}_{82}\mathrm{Pb}_{126}$ with a sharp fall-off. Likewise, the projected distributions onto the mass and charge axes shows a clear preference for cluster emission, as seen in the top panels of Figure 5.5.

As discussed in Chapter 2, the collective inertia can also have a large impact on the fission dynamics. Using the $\mathrm{UNEDF1_{HFB}}$ functional, we compared our result with the non-perturbative cranking ATDHFB inertia $\mathcal{M}^{\mathrm{A}}$ to the perturbative ATDHFB $\mathcal{M}^{\mathrm{AP}}$ (which appears smoothed-out compared to $\mathcal{M}^{\mathrm{A}}$) and perturbative GCM $\mathcal{M}^{\mathrm{GCM}}$ (which is smooth and also lower in magnitude than $\mathcal{M}^{\mathrm{A}}$ or $\mathcal{M}^{\mathrm{AP}}$ by roughly a factor of 1.5), which are often easier to use for large-scale calculations. The result, shown in the middle panels of Figure 5.5, show that the distribution has shifted slightly, but that $\mathcal{M}^{\mathrm{AP}}$ and $\mathcal{M}^{\mathrm{GCM}}$ give identical, or nearly-identical results. The smoothness of the perturbative inertias apparently allow fluctuations to drive the system to more extreme fragment configurations. This suggests that the magnitude of the inertia matters less than the topography for computing fission yields (though we note that this would not be true for calculating half-lives, which depend exponentially on the magnitude of the inertia).

We also vary the strength of fluctuations by adjusting the parameter η. Our starting point η_0 is taken from reference [28], where it was obtained by adjusting η to match the experimental fragment distribution of ${}^{294}\mathrm{Pu}$. Shown in the bottom panel of Figure 5.5, we

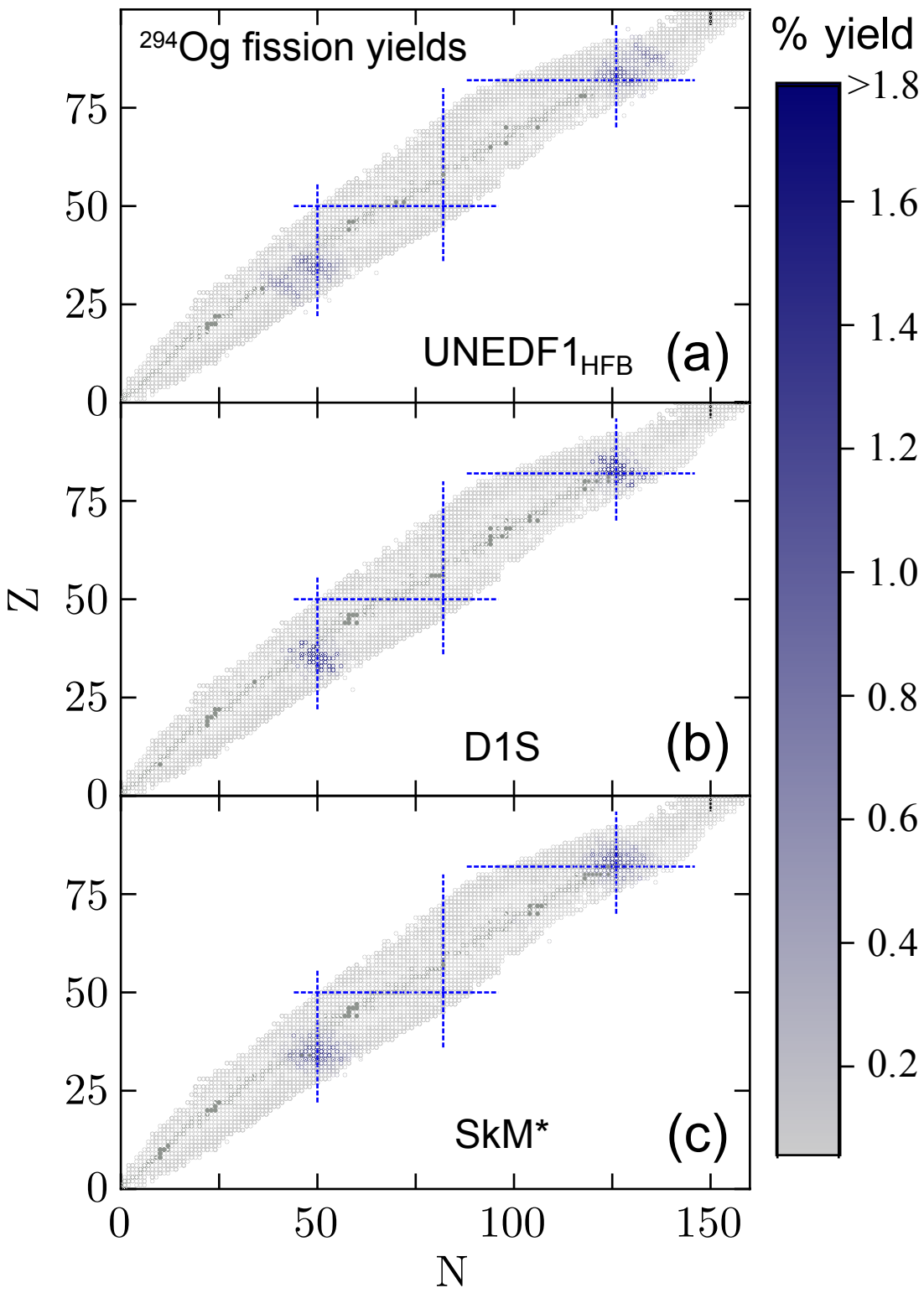

Figure 5.4: Fission fragment distributions for $^{294}_{118}\mathrm{Og}_{176}$ obtained in UNEDF1$_{\mathrm{HFB}}$ (a), D1S (b), and SkM* (c) EDFs using the non-perturbative cranking ATDHFB inertia and the baseline dissipation tensor η_0. Known isotopes are marked in grey [**?**]. Magic numbers 50, 82, and 126 are indicated by dotted lines.

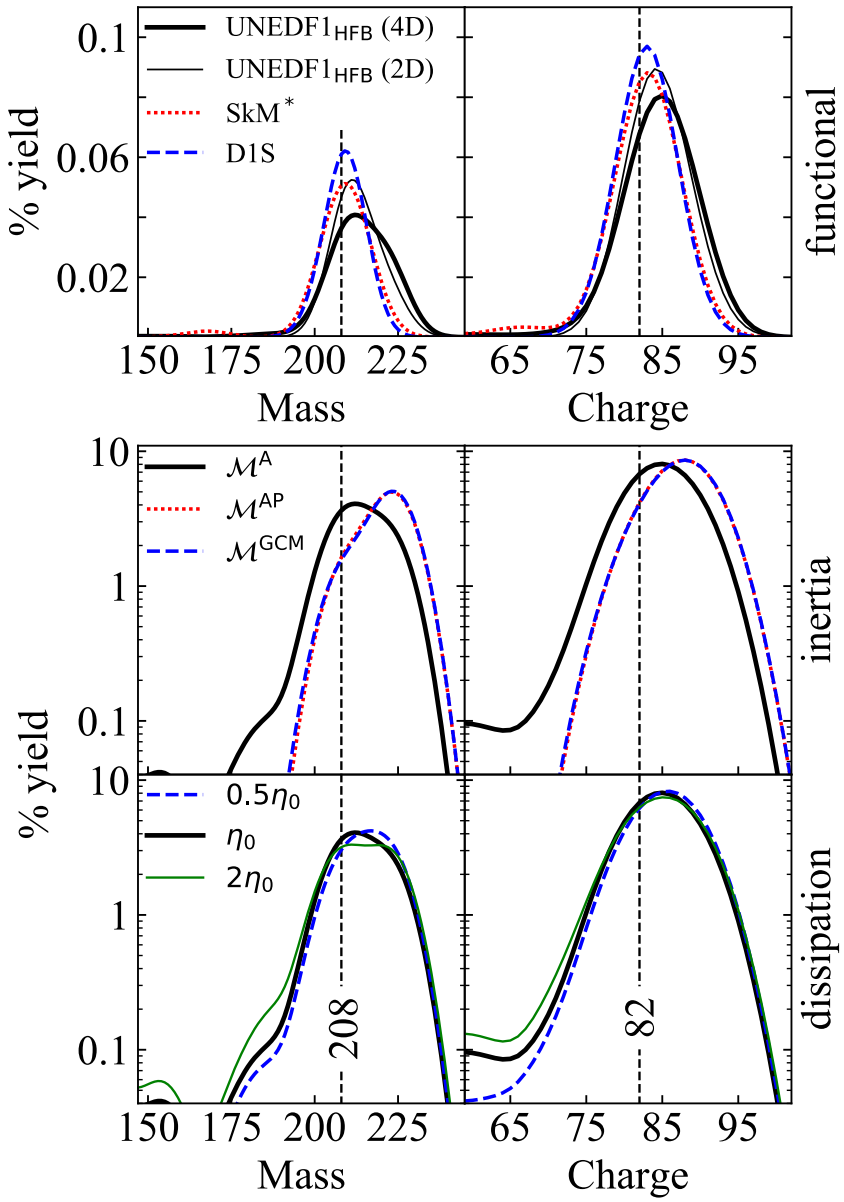

Figure 5.5: Upper panel: Predicted heavy fragment mass (left) and charge (right) yields of $^{294}_{118}\mathrm{Og}_{176}$ using different functionals (top, linear scale). Bottom panels: collective inertias and dissipation tensor strengths (in logarithmic scale). The baseline calculation was performed using the $\mathrm{UNEDF1_{HFB}}$ functional in a 4D space with non-perturbative cranking ATDHFB inertia and dissipation tensor strength η_0.

find that fluctuations do not affect the peak of the distribution, consistent with the results of Refs. [27, 70, 71]. The primary effect is in the tails.

5.3 Fragment formation in ^{294}Og

The Langevin dynamics approach is useful for calculating total yield distributions, but they do not offer much physical insight into the process of fragment formation. In order to better understand fragment formation for the most-probable fragments, we computed the nucleon localization function (section 2.1.4 and References [26, 27]) along the cluster emission path. This is shown in Figure 5.6, where it is compared to the fragments $^{208}_{82}\mathrm{Pb}_{126}$ and $^{86}_{36}\mathrm{Kr}_{50}$. We found that the lead prefragment is well-localized as early as just outside the outer turning line. The $N \approx 50$ neutrons belonging to krypton are also well-localized, but the $Z \approx 36$ protons are not, highlighting the importance of shell effects in prefragment formation.

In fact, we can leverage this insight to predict fission fragments as early as the outer turning line, resulting in a major reduction in total computing time because of the reduced PES. This is described in Appendix A.

5.4 Experimental efforts to find cluster emission in ^{294}Og

Perhaps the biggest uncertainty we'll see, or the biggest deviation from experiment, will be the distribution width. That's because we folded our Langevin results with a Gaussian function, the width of which was chosen rather arbitrarily to be $\sigma_A = 6, \sigma_Z = 4$. The values used in ^{240}Pu were 3 and 2, but the Q_N value they used to define scission was quite a bit smaller too. Since we had a much larger Q_N cutoff, we needed to account for larger particle number fluctuations. But these numbers were just kind of arbitrary. I'm not too worried

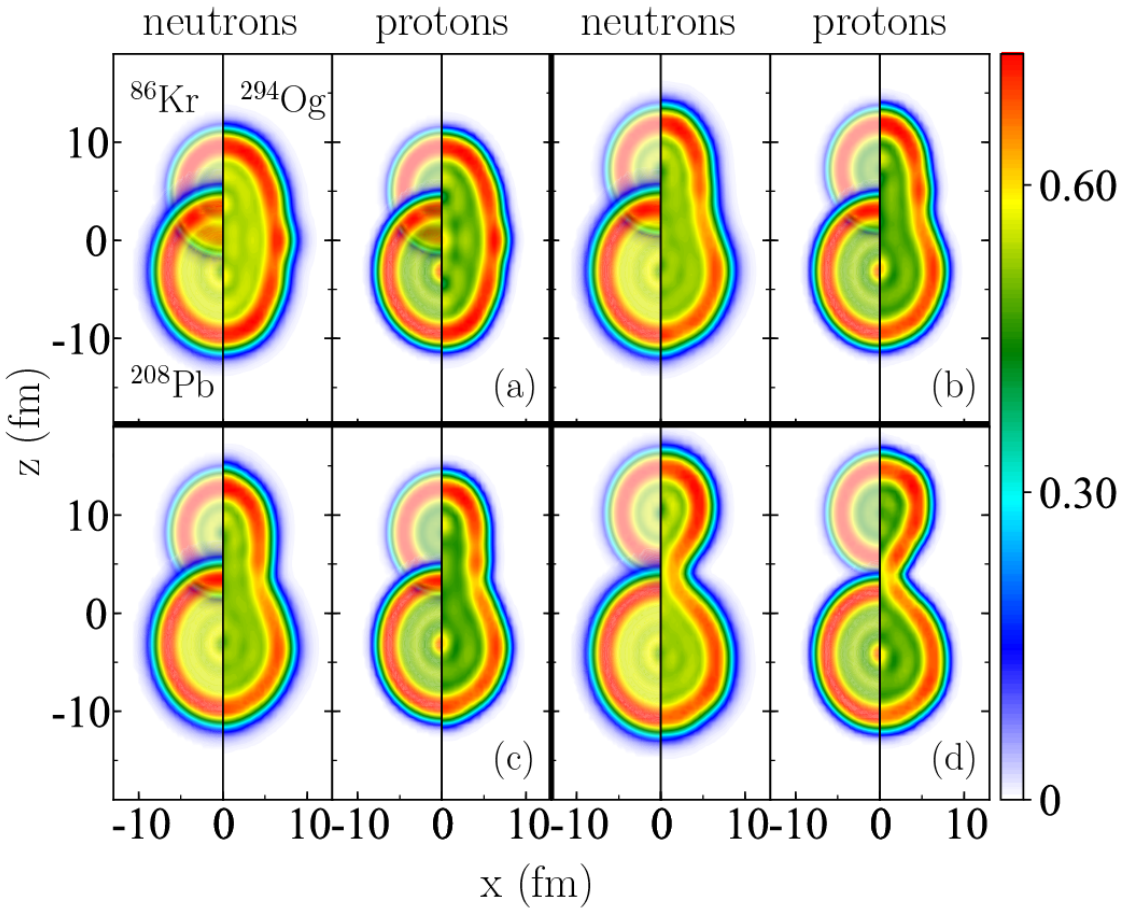

Figure 5.6: Nucleon localization functions for several deformed configurations of $^{294}_{118}\mathrm{Og}_{176}$. For comparison, localizations are shown for the fragments $^{208}_{82}\mathrm{Pb}_{126}$ and $^{86}_{36}\mathrm{Kr}_{50}$ on the left side of each subplot. The configurations shown correspond to Fig. 1 from the paper, with multipole moments (Q_{20}, Q_{30}) = (a) (75 b, 0); (b) (120 b, 17 $\mathrm{b}^{\frac{3}{2}}$); (c) (140 b, 24 $\mathrm{b}^{\frac{3}{2}}$); and (d) (264 b, 60 $\mathrm{b}^{\frac{3}{2}}$).

about this because the peak is the part that matters, and we clearly saw a peak at the cluster location.

The effort to detect cluster emission in superheavy elements is already underway. However, one of the biggest challenges standing in the way of observation of cluster emission from $^{294}_{118}\mathrm{Og}_{176}$ is the problem of statistics. There have only been 5 recorded instances of $^{294}_{118}\mathrm{Og}_{176}$, from the first observations in 2005 [72] to the most recent in [65].[1] To maximize the possibility of detecting SF events as they happen, there is some discussion in the experimental community about building an ionization chamber with the ability to distinguish fragments by their Z-value. This is discussed at some length in [65]:

"Among these SF events, there were signals correlated with incoming recoil-like signals within the time range of the 294Og half-life. We have inspected the possible assignment of some SF events to the fission of 294 Og. In the past, as well very recently, 294 Og was considered as a system consisting of doubly magic 208 Pb and singly magic N = 50, 86 Kr. These two components are well bound stable nuclei. One can envision that an asymmetric fission of 294 Og into 208 Pb and 86 Kr fragments might be somewhat enhanced.

"However, especially since the decay time of 294 Og is not sufficiently different from 258 No decay, one cannot make an assignment to 294 Og activity based only on the half-life of SF events. The energy of SF events vary, since we detect sometimes only a partial energy of fission fragments. Such events are more likely to arise from the SF activity produced in a multinucleon transfer involving the Cf isotope in the target. The indistinguishability of complete-fusion from transfer reaction products provides motivation for an ionization chamber, which would have a discrimination capability for the atomic number Z, placed before

[1] In fact, there were reports as early as 2004 [73] that there may have been detected instances of fission fragments resulting from the spontaneous fission of $^{294}_{118}\mathrm{Og}_{176}$, but these are unconfirmed.

the implantation Si counter. Construction and anticipated performance of such an ionization chamber based on gas electron multiplier (GEM) technology was recently discussed..."

Chapter 6

Fission in the r-process

6.1 The role of fission in the astrophysical r-process

One of the outstanding mysteries in astrophysics is the origin of heavy elements. It is thought that heavy elements are formed in a violent, neutron-heavy astrophysical scenario, such as a supernova or a neutron star merger, as light "seed" nuclei are rapidly bombarded by neutrons. This rapid neutron capture process, generally shortened to "r-process," increases the mass of seed nuclei until eventually they beta decay toward the valley of stability. This process is illustrated schematically in Figure 6.1.

Fission plays an important role in the r-process. The competition between neutron capture rates, fission rates, and other decays determines the direction in which the r-process proceeds. Fission also places an upper limit on the mass that can be produced in an r-process scenario, as fission lifetimes for heavy and superheavy isotopes become small enough to compete with the neutron flux of the environment around $N \approx 184$. Also, as will be discussed shortly, fissioning isotopes in this mass region are thought to lead to the rare earth peak around $A \approx 165$.

A related topic is the question of fission cycling. Once a heavy nucleus fissions, its fragments can then absorb more neutrons and make their way back up the r-process chain. Elemental abundance patterns in stars outside our solar system somewhat resemble that

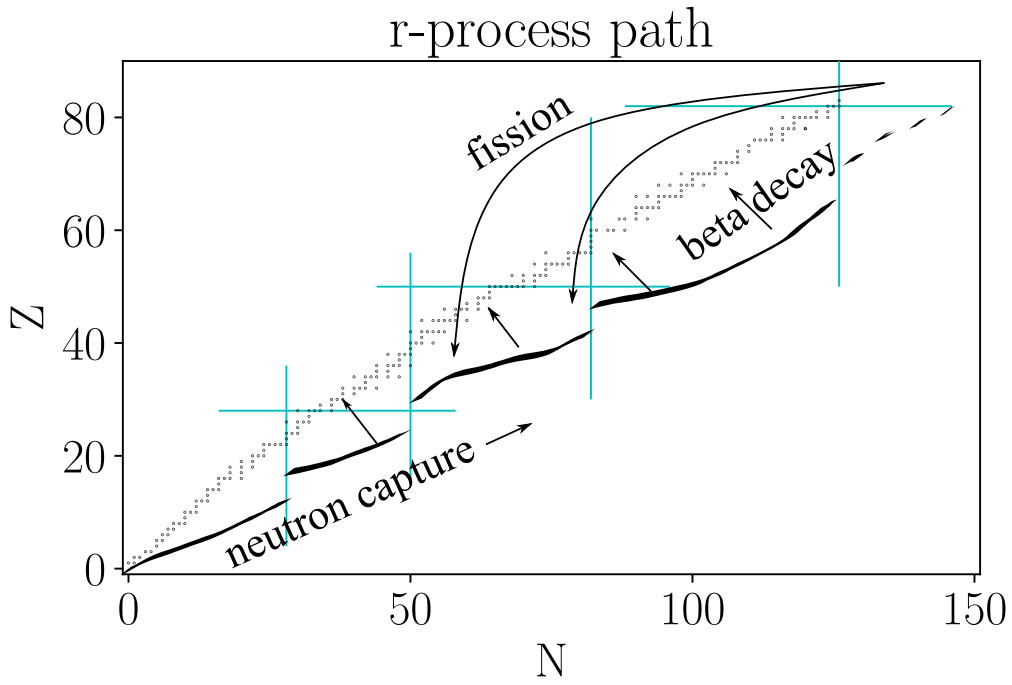

Figure 6.1: Schematic overview of the r-process. Neutron capture increases the mass of seed nuclei until they reach the drip line or decay, e.g. via beta decay or fission (spontaneous, beta-delayed, or neutron-induced).

of our own [74], and it has been suggested that fission cycling may be responsible for this "universality" of the r-process [75].

R-process network calculations combine nuclear physics inputs, such as decay lifetimes, capture cross sections, and fission fragment yields, with astrophysical inputs, such as temperature and neutron flux, to simulate the complex competition between neutron capture and various forms of nuclear decay. Such calculations require quality inputs from a variety of sources. In order to guide experimental and theoretical efforts and to reduce uncertainties in the abundance pattern, sensitivity studies (in which inputs are tweaked to measure their impact on the final yield) can estimate the impact of a particular set of observables, such as fission fragment yields, on the r-process abundance pattern.

Sensitivity studies indicate that fission yields primarily affect the abundance and location of the rare earth peak and the second r-process peak ($A \approx 100 - 160$) [76, 77]. This can

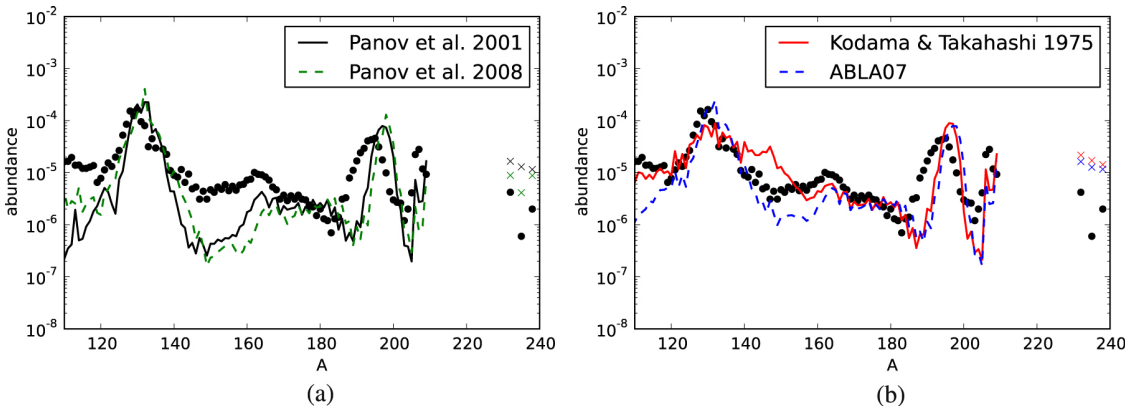

Figure 6.2: Quoting their caption: "Final abundances of the integrated ejecta around the second and third peak for an NSM (Korobkin et al. 2012; Rosswog et al. 2013) at a simulation time $t = 10^6$ s, employing the FRDM mass model combined with four different fission fragment distribution models (see the text). For reasons of clarity the results are presented in two graphs. The abundances for Th and U are indicated by crosses. In the left-hand panel the lower crosses belong to the Panov et al. (2008) model (dashed line), while the lower crosses in the right-hand panel belong to the ABLA07 distribution model (dashed line). The dots represent the solar r-process abundance pattern (Sneden et al. 2008)." [77]

be seen in Figure 6.2, in which four different sets of fission fragment yields were used to compute abundances. That this region should be sensitive to fission yields should come as no great surprise, since most fission fragments are likely to lie in the range $A \approx 100 - 160$.

In [78], the authors performed a sensitivity study in which, instead of assessing uncertainties, their goal was to isolate "hot spots" of nuclei that would have the greatest impact on the final r-process abundances. Four different mass models were used to estimate these hot spots; in Figure 6.3 the neutron-induced fission hot spots are shown, with the four different results superimposed on top of one another. We selected a few of these "hot spot" nuclei to analyze microscopically.

Figure 6.3 shows specifically neutron-induced fission; however, the phenomenological (GEF) yields that were used do not show a strong dependence on excitation energy for many nuclei of interest. Therefore, for simplicity, we simply calculate the spontaneous fission yields. A proper treatment of neutron-induced fission using a finite temperature

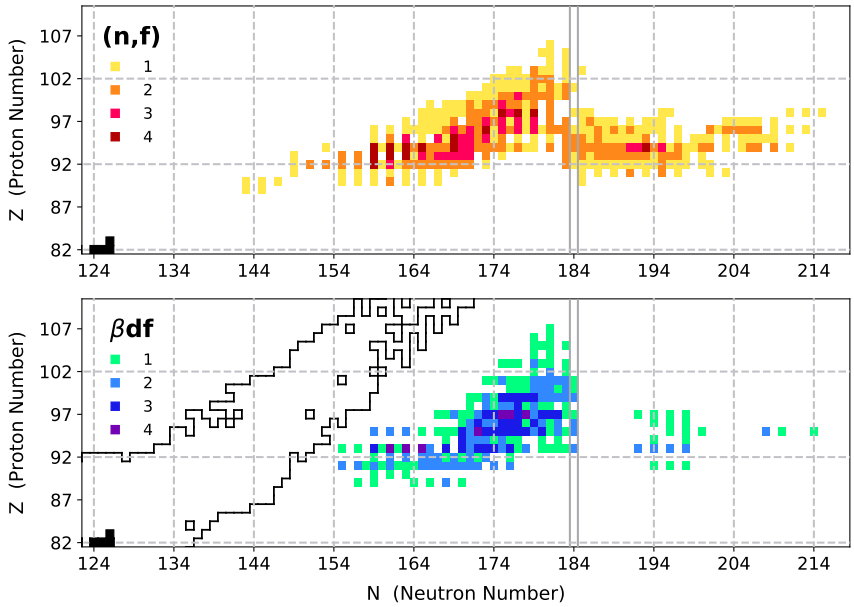

Figure 6.3: Heatmap showing isotopes whose fission yields are especially relevant to the r-process. This combines the results from four different mass models, and counts how many mass models found each isotope to be relevant (integrated fission flow above a certain threshold). [78]

formalism is being developed [46, 79, 80], but many challenges still remain (see Appendix, `\cite{cnr2018-proceedings}`).

6.2 Fission fragment yields for r-process nuclei

Using 6.3 as a guide, the isotopes ^{254}Pu, ^{264}Pu, ^{288}Pu, ^{270}Cm, and ^{276}Cf were selected for study. For each isotope, a 1D PES was calculated up to the outermost isomer state by constraining Q_{20} and leaving the other degrees of freedom unconstrained. Between the isomer state and the outer turning line, the PES was expanded to include Q_{30} in order to account for mass asymmetry between the fragments. The WKB method was used to estimate relative probabilities along the outer turning line, at which stage fragment pairs were identified using the localization-based method described in `\cite{locali, appendix}`.

The resulting distributions will be shown in Figure \ref{???} whenever I have them.

[Maybe the methods portion of this project, and/or the justification of the method, should be moved to another Appendix instead of the main body of the text. It's important, certainly, but it's not central to the narrative]

6.3 Kilonova and ^{254}Cf

An open questions about the r-process is where exactly it takes place. Core-collapse supernovae were a leading contender for years, but that hypothesis has recently fallen out of favor because of reasons \cite{???}. Bolstered by theoretical calculations \cite{???} and the neutron star merger event GW170817, neutron star mergers have become the site favored by many today. However, the results are far from conclusive, and stronger evidence is needed. The isotope $^{254}_{98}\mathrm{Cf}_{156}$ has been identified as a signature to help astronomers identify potential r-process sites.

It is suspected that the kilonova in a neutron star merger is produced by residual radioactivity as neutron-rich material produced in the merger decays toward stability. This material produces an observable light curve, which is one way to characterize the kilonova. The light curve will be dominated by alpha and beta decay events at early times, but if nuclei with spontaneous fission half-lives on the order of several days are produced in sufficient quantities, these would have a major impact on late-time heating in the kilonova, which in turn would affect the light curve. Thus, the shape of the light curve may indicate whether or not heavy, short-lived actinides were produced.

The question remains whether such nuclei exist which. Limiting ourselves to isotopes which have been experimentally measured, there are several which primarily undergo spon-

taneous fission and which may be produced in significant quantities in the r-process: several isotopes each of californium and fermium, plus ^{260}Md. However, most of the fermium and californium isotopes are too short-lived, and the population of ^{260}Md is highly model-dependent, leaving $^{254}_{98}\mathrm{Cf}_{156}$ as the most-likely candidate.

Perhaps you should cite [81], if no one else.

The effect of $^{254}_{98}\mathrm{Cf}_{156}$ on the heating and light curve depends on the energy released during fission, which in turn depends on the fragment yield it produces. Mass and kinetic energy distributions of $^{254}_{98}\mathrm{Cf}_{156}$ were actually measured in [82]. For some reason, though, Zhu considers that measurement "sparse" and they do some dressing up of it in their paper [81]. We decide to compute it microscopically using our Langevin approach, just to see what useful information we can add.

Chapter 7

Outlook

Having discussed several different results, it is worth taking some time to reflect.

The overarching goal of the project, in which this dissertation is a part, is to describe spontaneous fission observables in a fully self-consistent framework based on fundamental nuclear physics. At this stage, we are able to estimate half-lives and primary fragment distributions [to around X% accuracy, for the nuclei with which comparison to experiment is possible].

7.1 Perspectives for future model development

7.1.1 Numerical challenges

We can hope to achieve greater fidelity in our calculations by

We definitely need a better handle on the inertia. The perturbative inertia is easy to compute, but not terribly reliable. The non-perturbative inertia can certainly do better, but as it is computed now (using finite differences) it is subject to numerical artifacts and instabilities (dependent on the level of convergence of the individual densities, the coefficient multipliers, different basis sizes) as well as to actual physics, such as level crossings which manifest in projections from a higher-dimensional space. One tool that has been suggested which would eliminate the need for finite-difference derivatives is automatic differentiation

\cite{???}.

UNEDF1 seems to underestimate fission barrier heights (artificial though the concept may be; the main impact is probably that lifetimes are underestimated). It also turns out to be a headache to work with, making convergence quite a challenge sometimes (any cases in particular, like for highly-deformed or heavy or octupole-deformed nuclei or something?). Better functionals might hope to better capture the physics, and one can hope they are easier to work with. (here you could mention the DME EDFs; unfortunately, introducing density-dependence causes problems for beyond-mean field corrections)

The construction of a PES is fraught with ambiguities. Trying to reduce a complex system with hundreds of degrees of freedom into only a few collective coordinates creates artificial discontinuities and other artifacts, while at times missing important physics. Brute force computation with a larger number of collective coordinates (such as we did in Chapter 5) will become more accessible as computers continue to become more powerful. However, we might see a faster turnaround on our investment if we start using collective coordinates that better describe the physics of fission. For instance, a set of coordinates D, ξ was proposed as an alternative to the traditional Q_{20}, Q_{30} coordinates in [30], where D is the distance between prefragment centers of mass and $\xi = (A_R - A_L)/A$ characterizes the fragment asymmetry. Using these coordinates, the authors found that they were better able to describe scission configurations than if they had used multipole moments instead.

To that end, it is worth mentioning as well Fragment identification (our localization paper, Marc Verriere's method; you might also mention that this is not an issue in TDDFT, but there you've only got one single fragment pair)

7.1.2 Self-consistent stochastic dynamics

To make the calculations we've performed fully self-consistent, we will need to use a microscopic/self-consistent description for dissipation. This is the mechanism which exchanges between intrinsic and collective degrees of freedom, but we handle it in a very ad hoc way with parameters which are fitted instead of determined systematically through some theory. Solving this problem will probably help us with the energetics of fragments (TKE and E* at the same time!)

A proper understanding of the friction tensor (as it were) may also help with the calculation of neutron emissions, according to this: "The influence of friction on the fission rate was studied in papers [57, 58]. It was shown there that dissipative effects might lead to emission of more neutrons from fissioning nuclei than what is predicted by equilibrium statistical models." (`https://link.springer.com/article/10.1134%2FS1063779610020012`).

Some other papers you can look at for this might be `https://doi.org/10.1142/S0218301398000105`, `https://doi.org/10.1016/j.physletb.2007.09.072`, and `https://doi.org/10.1016/0375-9474(79)`

7.2 Perspectives for future physics applications

7.2.1 Half-lives

Although an approach was outlined for computing spontaneous fission half-lives in Chapter 2, no practical results have yet been obtained using this method. The biggest difficulty here is the exponential dependence of the half-life on the action, which is in turn a function of the potential energy, the collective inertia, and the zero-point energy. The numerical improvements outlined above will all serve to ameliorate the situation; additionally, there

are maybe better ways to compute E_0? `\cite{???}`

7.2.2 Predicting other experimental observables

Furthermore, there are more experimental observables that we should try to predict (refer to Andreyev's review to see what other observables can currently be measured). These include energetics (TKE and E*, for we have only begun to scratch the surface here), angular momentum, prompt neutron multiplicities (is that within the scope of these self-consistent models?), prompt neutron and gamma energy spectra (getting harder; these are usually handled via statistical models; see intro to [35] for some references), level densities?, and probably more but my mind is blanking. How to compute these in a self-consistent framework is still an open question. See also the outlook in Nicolas' review.

Some methods (such as Walid's, TDDFT, and possibly also this GCM method) are starting to estimate fragment energetics (kinetic and excitation energies). Down the line, there are others who try to predict neutron multiplicities and goodness knows what else using Hauser-Feshbach models and such (FREYA and more). These regions are still disconnected. Of course, these methods still need major refinements in order to better reflect experimental data. Some ideas currently in the pipeline for improving the models are:

7.2.3 Large-scale calculations with machine learning

Something that could be pretty doable and also moderately useful would be to use machine learning for fission yields to use in r-process network calculations. I got this idea from a guy at LLNL who gave a CMSE colloquium. He described a machine learning paradigm (he called it an "Elevated Model") in which they teach a deep learning network everything it

could possibly care to know about a particular model - essentially, creating an emulator of the model. Then you kind of snip off the last couple of layers of your network, and reteach it (holding all but those last two layers constant), this time using experimental data. So by now you've gotten most of the physics intuition built into your emulator through the model training, and then for the physical insight your model misses (and perhaps to help reduce overfitting), you've taught it where the emulator goes wrong and what to do about it.

How can this help us fission folks? Well, right now the r-process network folks in the FIRE collaboration are using the GEF model for fission fragments and whatnot. It's basically a black box of magic that is super-overfitted and no one is completely sure how it works. BUT it's the best they've got for fission yields all across the region of interest, so that's what they use. My thought is to take this as a starting point (our "model data"), and then use a combination of DFT calculations and also *actual* experimental data as our experimental data. This could be an interesting opportunity to utilize your 290Fm results, along with anything else you've worked on.

Samuel worries (and I think, with justification) that we might not see any substantial improvements because the GEF is already so heavily overfitted. That, and that it might take a really long time (Leo's concerns are similar, plus he is concerned about having enough training data to do anything meaningful). That is why I'm thinking through what would need to be done, step by step, just to get a feel for a timeline of feasibility:

- Finish a 290Fm calculation or something nearby, just to have at least *something* out there
- Figure out how to build a neural network where you can keep some layers fixed while selectively modifying others. I don't think that's something you could do in Scikit-

learn; that you'd probably have to build custom (though fortunately you've already got something that might work!). Or you might be able to use TensorFlow (or Keras)

- Determine what observables you'd like (and are able) to include in your evaluation. For sure the locations of the peaks. Maybe also the width? Can you predict a full distribution from the same NN, or do you have to create a different one for each?
- Run the GEF for as many nuclei as you want to include in your evaluation
- Collect theoretical+experimental data you'll use to train your improved model
- Set aside a training set (Ideally you should include something that GEF clearly gets wrong compared to experiment, if possible)

The nice thing about this idea is that it can easily be extended or improved. Maybe some day Peter Moller has calculations across the landscape. You could just swap out the GEF data for Peter Moller's. Basically, it's just glorified interpolation, taking advantage of cheap models and combining/folding those with the more expensive, but more sparse, DFT and experimental results.

However, just based on Figure 1 of [78] and the preliminary yields I have for 266Cm and 290Fm, it doesn't look like we'd be adding too much new information. It looks to me like they already got the basic shape of the yields, and I don't know if I'd do much better with the localization fragment ID approach I'd been considering using.

7.3 Review and conclusions

APPENDICES

Appendix A

Fragment Identification

A.1 Fragments and the Nucleon Localization Function

An improved scission criterion would go beyond simply counting the number of particles in the neck. To help with this, we have a tool at our disposal which helps us to understand correlations that affect fission dynamics. This is called the nucleon localization function, and it allows us to visualize the prefragment nuclear shell structure which largely determines the identity of fission fragments [26].

The nucleon localization function shows that some prefragments can be very well-formed even when the neck is large, while in another case the neck might be small but the prefragments, poorly-defined [27]. A better scission criterion should take into account, or at least be compatible with, the insights gained from the nucleon localization function. As noted in [83], fragment properties on either side of the scission line may differ drastically. This is because shell structure is not well-described geometrically. Our localization measure offers an alternative scheme for identifying fragments before the scission line (see [27]). Since it is based on the underlying quantum shells, it is less sensitive to fluctuations and particle rearrangements late in the evolution.

A.2 The problem of scission

For practical reasons we are limited to describing complicated shapes in terms of just a few parameters, leading to uncertainty in the fragment properties. In particular, the part of the process at which the neck snaps and one nucleus becomes two, called scission, is not well-defined in static approaches.

Many times in static approaches, including the results shown in this dissertation so far, scission is frequently characterized by a single number such as Q_N, which approximately corresponds to the number of particles in the neck. When that number falls below a certain predefined threshold, we say that the nucleus has scissioned. Fragments are identified and one can try to estimate the strength of the repulsive interaction forcing the fragments apart. Of course, as discussed by Younes and Gogny in [84**?**], wavefunctions corresponding to individual nucleons may extend into the spatial region of the opposite fragment.

This can be understood with an analogy: suppose we stretch a nucleus until a neck forms, and then we use a butcher knife to lop the two fragments apart. This works reasonably well for estimating fragment mass and charge, but it is very poor when it comes to estimating the relative energy of the fragments. To estimate fragment kinetic and excitation energies, one needs to carefully and delicately peel the interlocking fragments apart with a scalpel, or a proper accounting of entanglement and other many-body correlations.

Essentially what we show is that Q_N is meaningless, and that any static definition of scission is going to need to account for the actual configuration of the system.

A.3 Prefragment shell structure

A common theme in all of this has been the importance of the underlying shell structure of the prefragments. Shell energy corrections were found to be important in ${}^{178}_{78}\mathrm{Pt}_{100}$ and ${}^{180}_{80}\mathrm{Hg}_{100}$; cluster formation in ${}^{294}_{118}\mathrm{Og}_{176}$ was clearly influenced by the shell structure of the fragments; and the same may or may not be the case for ${}^{254}_{98}\mathrm{Cf}_{156}$. Let's discuss this.

We used localizations to visualize the internal/intrinsic shell structure inside nuclei, and we were able to see that this structure was sometimes intact early in the evolution, at times as far back as the outer turning line. And actually, this kind of makes sense. From just energetics alone, a nucleus on the outer turning line is just as happy (or just as stable, or just as settled) as a nucleus in the ground state. In some sense, it is formed. The difference now is just that the configuration it's in is now unstable due to Coulomb. The two halves, which are kind of maybe happy from a nuclear physics perspective, are pushing apart from the Coulomb repulsion. So that still has to be carried out, but the bulk of the physics might already be done at this point - though not necessarily. It *could* be that the fragments are well-formed and just pushing apart, but that may not be the case. It's like a divorce: sometimes the two have drifted so far apart, or are so well-defined and incompatible as individuals that the divorce is simple and relatively straightforward. Other times, it is a mess trying to sort out who gets what, and the two parties are fundamentally-changed by the proceedings.

I don't have any strong objections to Scamps and Simenel's octupole paper. In fact, to me it kind of makes sense: we've been saying, after all, that it's the shell structure of the deformed prefragments which determine scission, and not necessarily the final fragments themselves. That's really the whole idea behind the localization paper: we're seeing that, at least in some cases, the shell structure is pretty well intact early in the evolution, and that

those prefragments drive the system to scission with some shuffling of the neck nucleons at scission. All they're saying is that those neck nucleons will affect the shell structure of the prefragments, and just based on the kinds of shapes that the system will take (small neck connecting two elongated or spherical fragments), the prefragments have a strong octupole moment (regardless of whether the fragments are elongated or spherical). So it shouldn't be the spherical magic numbers we worry about, but the deformed (in this case, octupole-deformed) magic numbers.

I feel like it shouldn't be too terrible to investigate this claim. What if we constrained the multipole moment(s) that correspond(s) to octupole-deformed fragments (perhaps Q_{50})? I think this parameter might be included in Peter Moller's model, but not in ours.

A.4 Isospin transport

We're assuming that the parent nucleus gets to however it gets at the OTL (maybe it just happens to oscillate into that configuration randomly one day, and it feels reasonably stable there (per Witek's deformed harmonic oscillator paper)), and now we're trying to argue about how the neck nucleons will flow to rearrange themselves. So we're already imposing the assumption that the nucleons *will* flow from the neck to the fragments (and indeed, that at least seems to be what happens based on the success of this type of model so far).

This is indeed in contradiction with Scamps and Simenel's paper, because they essentially claim that once you get to that OTL configuration, the octupole deformation of the fragments (created by a spherical-ish prefragment with neck nucleons on the side, giving it a non-zero Q30) is sufficiently strong to snap the neck and let the fragments go on their merry way, octupole-deformed and everything. On the other hand, we're saying that instead, it's

just a lucky coincidence that the fragments are stable in an octupole-deformed configuration because they're not going to stay that way once the neck nucleons flow to their final destination.

There are these isospin transport papers essentially describe the flow of isospin and density in terms of the chemical potential and gradients. Nucleons will flow based on the chemical potential properties of the system, or in other words, to minimize the binding energy of the system. In general, that means you'll see a flow of neck nucleons in such a way as to bring the final fragments as [jointly] close to stability as possible.

The density gradient terms will lead to a flow of nucleons from prefragments to neck (with apparently a greater effect on neutrons than on protons).

Jhilam sent a couple of experimental papers where alpha clusters were observed emitting from the neck (perpendicular to the momenta of the fragments). Might this localization tool be used to later help model neutron and alpha emission?

Appendix B

Temperature-Dependent ATDHFB Collective Inertia

Be sure to discuss the complications which arise in the finite temperature formalism, as promised in Chapter 3. In essence, you end up dividing by terms which are very small. You can avoid dividing by zero by introducing a cutoff. If the cutoff is too large, you lose some of the data in the tail. If the cutoff is too small, you divide by numbers that are smaller than the noise in the density. There are actual numbers in your dudeman4 Google Drive, in a file called Inertia Tensor Convergence.

B.1 Fission at finite temperature

Everything which was shown in this dissertation assumed that the system was maintained at temperature $T = 0$ and the nucleus behaved as a superfluid below the Fermi surface. However, in many environments (such as a neutron star merger or a nuclear blast) there may be quite a bit of excitation energy imparted to the system, which would raise the temperature above the Fermi surface. Additionally, and more relevant to this dissertation, a finite-temperature formalism is used to describe neutron-induced fission in, e.g. [46]. In the $T \neq 0$ case, pairs may be broken and various excited states are accessible, resulting in changes to the the potential energy surface and, as will be shown in this chapter, the

collective inertia.

A lot of these ideas I'm getting from [80] as well as Nicolas' own temperature-dependent HFB notes.

B.2 Finite-temperature density

As in any statistical theory, one first must determine which sort of ensemble properly describes the system. Nuclei are systems which have a conserved number of particles; however, HFB theory explicitly breaks particle number symmetry because of the Bogoliubov transformation. In principle we should perhaps use a microcanonical ensemble to describe a nucleus as a closed, isolated system, but that turns out to be challenging to solve because it requires a full knowledge of the eigenspectrum of the nucleus. Using the particle non-conserving quirk of HFB theory, we wiggle our way out of this hairiness[1] to instead describe our system using the grand canonical ensemble, and this approach turns out to be tractable.

Moving forward by minimizing the grand potential Ω gives us for the density:

$$\hat{D} = \frac{1}{Z} e^{-\beta\left(\hat{H}-\mu\hat{N}\right)} \tag{B.1}$$

with associated partition function

$$Z = Tr\left[e^{-\beta\left(\hat{H}-\mu\hat{N}\right)}\right] \tag{B.2}$$

Moving toward our particular choice of mean-field Hamiltonian, we substitute some one-

[1] You can wave your hands here and say that finite temperatures let you break superfluid pairs, and so the number of "quasiparticles" (which, you could argue, might have referred to pairs previously but might now be extended to also include individual, unpaired particles) can change.

body operator for the exponent:

$$\hat{D}_{HF} = \frac{1}{Z} e^{-\beta \hat{K}}, Z = Tr\left[e^{-\beta \hat{K}}\right] \tag{B.3}$$

where in the simple Hartree-Fock case, $\hat{K} = \sum_{ij} K_{ij} c_i^\dagger c_j$ (in the HFB case, $\hat{K}$ is a sum of all different one-body operator types, but it's the same basic idea).

Defining the HF density matrix $\rho_{ij} = Tr\left[\hat{D}_{HF} c_j^\dagger c_i\right]$, we can show the following useful correspondence relations:

$$\rho = \frac{1}{1 + e^{\beta \hat{K}}} \tag{B.4}$$

$$Tr\left[\hat{D}_{HF} \hat{A}\right] = tr\left[\rho \hat{A}\right] = \sum_{ij} \rho_{ij} \hat{A}_{ij} \tag{B.5}$$

where $\hat{A}$ is an arbitrary operator in the single-particle basis. Similar things happen for the HFB case. At the end of the day in HFB, things work out to be pretty similar to the way they were before (see the full derivation in [85]), except the density in the quasiparticle basis is replaced by

$$\mathcal{R} = \begin{pmatrix} 0 & 0 \\ 0 & 1 \end{pmatrix} \rightarrow \begin{pmatrix} f & 0 \\ 0 & 1 - f \end{pmatrix} \tag{B.6}$$

with the Fermi factor f given by $f_\mu = \frac{1}{1+e^{\beta E_\mu}}$.

B.3 Temperature-Dependent ATDHFB

Let us quickly review the essence of Time-Dependent Hartree-Fock-Bogoliubov (TDHFB). The fundamental assumption of TDHFB is that a system which is a Slater determinant at time $t = 0$ and which is then allowed to evolve in time will remain a Slater determinant at all times t. This assumption allows us to write to TDHFB equation:

$$i\hbar\dot{\mathcal{R}} = [\mathcal{H}, \mathcal{R}] \tag{B.7}$$

where in the single-particle basis

$$\tilde{\mathcal{H}} = \begin{pmatrix} h - \lambda & \Delta \\ -\Delta^* & -h^* + \lambda \end{pmatrix}, \qquad \tilde{\mathcal{R}} = \begin{pmatrix} \rho & \kappa \\ -\kappa^* & 1 - \rho^* \end{pmatrix} \tag{B.8}$$

The *additional* assumption that collective motion is slow compared to single particle motion of the system is called the *adiabtic approximation*, and the consequent model is called Adiabatic Time-Dependent Hartree-Fock-Bogoliubov (ATDHFB). Historically, the reason for this assumption comes from microscopic-macroscopic models of nuclear fission, where the dynamics of the system are described by a few collective shape variables and their derivatives (analogous to coordinates and velocities). The adiabatic approximation is implicit in this assumption. ATDHFB provides the bridge for bringing this useful framework into a self-consistent, fully-microscopic picture.

Once the system is described in terms of collective coordinates and velocities, the energy can be expressed as the sum of a "potential" term (which depends on the coordinates) and a "kinetic" term (which depends on the velocities). Our goal is to understand the kinetic part of the energy, which in some sense describes the dynamics of a deformed nucleus, in terms of

the first few multipole moments of the nucleus. A key component of this will be the inertia tensor $\mathcal{M}$, which plays the role of the "mass": $E_{kin} \sim \frac{1}{2}\mathcal{M}\dot{q}^2$

B.3.1 Review of ATDHFB

With the adiabatic assumption in place, we can write the density as an expansion around some time-even zeroth-order density:

$$\mathcal{R}(t) = e^{i\chi(t)}\mathcal{R}_0(t)e^{-i\chi(t)} \tag{B.9}$$

$$= \mathcal{R}_0 + \mathcal{R}_1 + \mathcal{R}_2 + \dots \tag{B.10}$$

where χ is assumed to be "small" (which is explained more rigorously in [86]) and

$$\mathcal{R}_1 = i\left[\chi, \mathcal{R}_0\right] \tag{B.11}$$

$$\mathcal{R}_2 = \frac{1}{2}\left[\left[\chi, \mathcal{R}_0\right], \chi\right] \tag{B.12}$$

The HFB matrix, being a function of $\mathcal{R}$, is likewise expanded:

$$\mathcal{H} = \mathcal{H}_0 + \mathcal{H}_1 + \mathcal{H}_2 + \dots \tag{B.13}$$

and together $\mathcal{R}$ and $\mathcal{H}$ are plugged into the TDHFB equation B.7. Gathering terms in powers of χ:

$$i\hbar\dot{\mathcal{R}}_0 = [\mathcal{H}_0, \mathcal{R}_1] + [\mathcal{H}_1, \mathcal{R}_0] \tag{B.14}$$

$$i\hbar\dot{\mathcal{R}}_1 = [\mathcal{H}_0, \mathcal{R}_0] + [\mathcal{H}_0, \mathcal{R}_2] + [\mathcal{H}_1, \mathcal{R}_1] + [\mathcal{H}_2, \mathcal{R}_0] \tag{B.15}$$

These two equations are the ATDHFB equations. They can be solved self-consistently to find both χ and $\mathcal{R}_0$; however, this is rarely done in practice. A more common trick is to exploit the fact that solutions to the ATDHFB equations are (by design) *close* to true HFB solutions. One can then take an HFB solution and compute its time derivative by the first ATDHFB equation B.14 to get ATDHFB-like behavior without going through the full trouble of ATDHFB.

One nice feature of using true HFB solutions instead of ATDHFB solutions is that the matrix $\mathcal{H}_0$ is diagonal in the HFB basis.

Finally, the total energy of the system is found to be

$$E(\mathcal{R}) = E_{HFB} + \frac{1}{2}\mathrm{Tr}\left(\mathcal{H}_0\mathcal{R}_1\right) + \frac{1}{2}\mathrm{Tr}\left(\mathcal{H}_0\mathcal{R}_2\right) + \frac{1}{4}\mathrm{Tr}\left(\mathcal{H}_1\mathcal{R}_1\right) \tag{B.16}$$

The "kinetic energy" of the system is given by the latter two terms, which (as we'll show explicitly in a moment), are both second order in χ.

B.3.2 Relation between χ and $\dot{\mathcal{R}}$

Eventually we'll want to express the energy in terms of the multipole moments q and their derivatives, but for now we will content ourselves with expressing the energy in terms of $\mathcal{R}$ and $\dot{\mathcal{R}}$.

Working in the HFB quasiparticle basis, we have (at finite temperatures)

$$\mathcal{H}_0 = \begin{pmatrix} E & 0 \\ 0 & -E \end{pmatrix}, \qquad \mathcal{R}_0 = \begin{pmatrix} f & 0 \\ 0 & 1-f \end{pmatrix} \tag{B.17}$$

Note that the block matrices E and f are both diagonal. In this same basis, we can also divide the perturbation matrix χ and the first-order energy $\mathcal{H}_1$ in the same block matrix form:

$$\chi = \begin{pmatrix} \chi^{11} & \chi^{12} \\ \chi^{21} & \chi^{22} \end{pmatrix}, \qquad \mathcal{H}_1 = \begin{pmatrix} \mathcal{H}_1^{11} & \mathcal{H}_1^{12} \\ \mathcal{H}_1^{21} & \mathcal{H}_1^{22} \end{pmatrix} \tag{B.18}$$

Ultimately, by combining these with equations B.11, B.12, and B.14, we arrive at the result:

$$\begin{aligned}
\hbar\dot{\mathcal{R}}^{11}_{(0),ab} &= (E_a - E_b)(f_b - f_a)\chi^{11}_{ab} + (f_b - f_a)\mathcal{H}^{11}_{(1),ab} \\
\hbar\dot{\mathcal{R}}^{12}_{(0),ab} &= (E_a + E_b)\left(1 - (f_a + f_b)\right)\chi^{12}_{ab} + \left(1 - (f_a + f_b)\right)\mathcal{H}^{12}_{(1),ab} \\
\hbar\dot{\mathcal{R}}^{21}_{(0),ab} &= (E_a + E_b)\left(1 - (f_a + f_b)\right)\chi^{21}_{ab} - \left(1 - (f_a + f_b)\right)\mathcal{H}^{21}_{(1),ab} \\
\hbar\dot{\mathcal{R}}^{22}_{(0),ab} &= (E_a - E_b)(f_b - f_a)\chi^{22}_{ab} - (f_b - f_a)\mathcal{H}^{22}_{(1),ab}
\end{aligned} \tag{B.19}$$

It is common (the so-called "cranking approximation") to assume that changes in the density have approximately no effect on the mean field, in which case these relations reduce to

$$
\begin{aligned}
\hbar\dot{\mathcal{R}}^{11}_{(0),ab} &= (E_a - E_b)(f_b - f_a)\chi^{11}_{ab} \\
\hbar\dot{\mathcal{R}}^{12}_{(0),ab} &= (E_a + E_b)\left(1 - (f_a + f_b)\right)\chi^{12}_{ab} \\
\hbar\dot{\mathcal{R}}^{21}_{(0),ab} &= (E_a + E_b)\left(1 - (f_a + f_b)\right)\chi^{21}_{ab} \\
\hbar\dot{\mathcal{R}}^{22}_{(0),ab} &= (E_a - E_b)(f_b - f_a)\chi^{22}_{ab}
\end{aligned}
\tag{B.20}
$$

Sanity Check: In the $T = f = 0$ case, the ^{11} and ^{22} terms vanish completely and we are left with the familiar [zero-temperature] ATDHFB equations:

$$\hbar\dot{\mathcal{R}}^{12}_{(0),ab} = (E_a + E_b)\chi^{12}_{ab} + \mathcal{H}^{12}_{(1),ab} \tag{B.21}$$

$$\hbar\dot{\mathcal{R}}^{21}_{(0),ab} = (E_a + E_b)\chi^{21}_{ab} - \mathcal{H}^{21}_{(1),ab} \tag{B.22}$$

Another thing we must be careful of is the case of degenerate states. In such an event, $E_a = E_b$ and $f_a = f_b$, leading again to $\dot{\mathcal{R}}^{11}_{(0),ab} = \dot{\mathcal{R}}^{22}_{(0),ab} = 0$ (but I emphasize that this is only for this particular pair of states $|a\rangle$ and $|b\rangle$).

A third, rather pedantic case to be aware of is the example of a two-state system. In that case, $f_a + f_b = 1$ and then the opposite happens; namely, $\dot{\mathcal{R}}^{12}_{(0),ab} = \dot{\mathcal{R}}^{21}_{(0),ab} = 0$ while $\dot{\mathcal{R}}^{11}_{(0),ab} \neq 0, \dot{\mathcal{R}}^{22}_{(0),ab} \neq 0$

B.3.3 Kinetic Energy at Finite Temperature

As mentioned previously, the expression for the "kinetic" energy of the system is given by:

$$E_{kin}(\mathcal{R}) = \frac{1}{2}\mathrm{Tr}\left(\mathcal{H}_0\mathcal{R}_2\right) + \frac{1}{4}\mathrm{Tr}\left(\mathcal{H}_1\mathcal{R}_1\right) \tag{B.23}$$

B.3.3.1 Term proportional to $\mathcal{R}_2$

It can be shown that

$$\mathrm{Tr}\left(\mathcal{H}_0\mathcal{R}_2\right) = \frac{1}{2}\mathrm{Tr}\left(\left[\chi, \mathcal{H}_0\right]\left[\chi, \mathcal{R}_0\right]\right) \tag{B.24}$$

which leads to

$$[\chi, \mathcal{H}_0] = \begin{pmatrix} [\chi^{11}, E] & -\left\{\chi^{12}, E\right\} \\ \left\{\chi^{21}, E\right\} & -[\chi^{22}, E] \end{pmatrix}, \qquad [\chi, \mathcal{R}_0] = \begin{pmatrix} [\chi^{11}, f] & \chi^{12} - \left\{\chi^{12}, f\right\} \\ -\chi^{21} + \left\{\chi^{21}, f\right\} & -[\chi^{22}, f] \end{pmatrix} \tag{B.25}$$

$$\begin{aligned} \mathrm{Tr}\left(\mathcal{H}_0\mathcal{R}_2\right) = \frac{1}{2}\mathrm{Tr}\Big([\chi^{11}, E][\chi^{11}, f] + \Big\{\chi^{12}, E\Big\}\left(\chi^{21} - \{\chi^{21}, f\}\right) \\ + \Big\{\chi^{21}, E\Big\}\left(\chi^{12} - \{\chi^{12}, f\}\right) + [\chi^{22}, E][\chi^{22}, f]\Big) \end{aligned} \tag{B.26}$$

Since E and f are diagonal, we can simplify expressions involving commutators and anticommutators. If A is an arbitrary matrix and D is diagonal, then

$$[A, D]_{\mu\nu} = (D_\nu - D_\mu)A_{\mu\nu} \tag{B.27}$$

$$\{A, D\}_{\mu\nu} = (D_\mu + D_\nu)A_{\mu\nu} \tag{B.28}$$

$$A_{\mu\nu} - \{A, D\}_{\mu\nu} = (1 - D_\mu - D_\nu)A_{\mu\nu} \tag{B.29}$$

Then this energy term becomes

$$\frac{1}{2}\mathrm{Tr}\left(\mathcal{H}_0\mathcal{R}_2\right) = \frac{1}{4}\Big[(E_b - E_a)(f_a - f_b)\chi^{11}_{ab}\chi^{11}_{ba} + (E_a + E_b)(1 - f_a - f_b)\chi^{12}_{ab}\chi^{21}_{ba} \tag{B.30}$$

$$+(E_a + E_b)(1 - f_a - f_b)\chi^{21}_{ab}\chi^{12}_{ba} + (E_b - E_a)(f_a - f_b)\chi^{22}_{ab}\chi^{22}_{ba}\Big] \tag{B.31}$$

If you wanted to get *really* crazy (and we'll see in a bit why this might actually be okay), you could even throw in some extra delta functions to get this:

$$\frac{1}{2}\mathrm{Tr}\left(\mathcal{H}_0\mathcal{R}_2\right) = \frac{1}{4}\Big[(E_b - E_a)(f_a - f_b)\delta_{a\alpha}\delta_{b\beta}\chi^{11}_{\alpha\beta}\chi^{11}_{ba} + (E_a + E_b)(1 - f_a - f_b)\delta_{a\alpha}\delta_{b\beta}\chi^{12}_{\alpha\beta}\chi^{21}_{ba} \tag{B.32}$$

$$+(E_a + E_b)(1 - f_a - f_b)\delta_{a\alpha}\delta_{b\beta}\chi^{21}_{\alpha\beta}\chi^{12}_{ba} + (E_b - E_a)(f_a - f_b)\delta_{a\alpha}\delta_{b\beta}\chi^{22}_{\alpha\beta}\chi^{22}_{ba}\Big] \tag{B.33}$$

Note that this now has the general form

$$\frac{1}{2}\mathrm{Tr}\left(\mathcal{H}_0\mathcal{R}_2\right) = \bar{\mathcal{M}}'^{11,11}_{\alpha\beta ab}\chi^{11}_{\alpha\beta}\chi^{11}_{ba} + \bar{\mathcal{M}}'^{12,21}_{\alpha\beta ab}\chi^{12}_{\alpha\beta}\chi^{21}_{ba} + \bar{\mathcal{M}}'^{21,12}_{\alpha\beta ab}\chi^{21}_{\alpha\beta}\chi^{12}_{ba} + \bar{\mathcal{M}}'^{22,22}_{\alpha\beta ab}\chi^{22}_{\alpha\beta}\chi^{22}_{ba} \tag{B.34}$$

where everything that isn't a χ has been absorbed into a single coefficient.

Pausing for a moment to reflect on what has just happened: Remember that the goal all along has been to treat this piece of the energy as sort of a "kinetic energy term" describing motion in a space of collective shape deformation coordinates. Then just now we found that,

sure enough, we can factor this particular chunk into something that looks *kind of* like $\frac{1}{2}mv^2$. And we already know from B.20 that χ is related to $\dot{\mathcal{R}}_0$. Eventually we'll try to relate $\dot{\mathcal{R}}_0$ to the collective shape coordinates $\dot{q}$, but first let's see if we can't get the other piece of the kinetic energy into the same form.

B.3.3.2 Term proportional to $\mathcal{R}_1$

Recall that $\mathcal{R}_1 = i\,[\chi, \mathcal{R}_0]$; then we can almost copy from equation B.26 of the previous section:

$$\begin{aligned}\frac{1}{4}\mathrm{Tr}\,(\mathcal{H}_1\mathcal{R}_1) &= \frac{i}{4}\mathrm{Tr}\,\Big(\mathcal{H}_1^{11}[\chi^{11}, f] - \mathcal{H}_1^{12}(\chi^{21} - \{\chi^{21}, f\}) \\ &\qquad +\mathcal{H}_1^{21}(\chi^{12} - \{\chi^{12}, f\}) - \mathcal{H}_1^{22}[\chi^{22}, f]\Big) \\ &= \frac{i}{4}\Big(\mathcal{H}^{11}_{(1),ab}(f_a - f_b)\chi^{11}_{ba} - \mathcal{H}^{12}_{(1),ab}(1 - f_a - f_b)\chi^{21}_{ba} \\ &\qquad +\mathcal{H}^{21}_{(1),ab}(1 - f_a - f_b)\chi^{12}_{ba} - \mathcal{H}^{22}_{(1),ab}(f_a - f_b)\chi^{22}_{ba}\Big) \end{aligned} \tag{B.35}$$

But what are those $\mathcal{H}^1$ terms? Since the interaction is known in the single-particle basis, we'll have to transform our density into the single-particle basis $\mathcal{R}_1 \to \tilde{\mathcal{R}}_1$, evaluate $\tilde{\mathcal{H}}_1$ (which depends on $\tilde{\mathcal{R}}_1$) in this basis, and then transform the result back into the quasiparticle basis $\tilde{\mathcal{H}}_1 \to \mathcal{H}_1$

$$\tilde{\mathcal{R}}_1 = \begin{pmatrix} \rho_1 & \kappa_1 \\ -\kappa_1^* & -\rho_1^* \end{pmatrix} = i \begin{pmatrix} U & V^* \\ V & U^* \end{pmatrix} \begin{pmatrix} [\chi^{11}, f] & \chi^{12} - \{\chi^{12}, f\} \\ -\chi^{21} + \{\chi^{21}, f\} & -[\chi^{22}, f] \end{pmatrix} \begin{pmatrix} U^\dagger & V^\dagger \\ V^T & U^T \end{pmatrix} \tag{B.36}$$

$$\Rightarrow \quad \rho_1 = i\left(U[\chi^{11},f]U^\dagger + U\left(\chi^{12} - \left\{\chi^{12},f\right\}\right)V^T - V^*\left(\chi^{21} - \left\{\chi^{21},f\right\}\right)U^\dagger - V^*[\chi^{22},f]V^T\right) \tag{B.37}$$

$$\kappa_1 = i\left(U[\chi^{11},f]V^\dagger + U\left(\chi^{12} - \left\{\chi^{12},f\right\}\right)U^T - V^*\left(\chi^{21} - \left\{\chi^{21},f\right\}\right)V^\dagger - V^*[\chi^{22},f]U^T\right) \tag{B.38}$$

In the single-particle basis, we can compute the interaction mean field $\Gamma_{(1),ij} = \bar{V}_{ikjl}\rho_{(1),lk}$ and the pairing field $\Delta_{(1),ij} = \frac{1}{2}\bar{V}_{ijkl}\kappa_{(1),kl}$:

$$\Gamma_{(1),ij} = \bar{v}_{ikjl}\rho_{(1),lk} \tag{B.39}$$

$$= i\bar{v}_{ikjl}\left(U_{l\alpha}[\chi^{11},f]_{\alpha\beta}U^\dagger_{\beta k} + U_{l\alpha}\left(\chi^{12} - \left\{\chi^{12},f\right\}\right)_{\alpha\beta}V^T_{\beta k}\right. \tag{B.40}$$

$$\left. -V^*_{l\alpha}\left(\chi^{21} - \left\{\chi^{21},f\right\}\right)_{\alpha\beta}U^\dagger_{\beta k} - V^*_{l\alpha}[\chi^{22},f]_{\alpha\beta}V^T_{\beta k}\right) \tag{B.41}$$

$$\Delta_{(1),ij} = \frac{1}{2}\bar{v}_{ijkl}\kappa_{(1),kl} \tag{B.42}$$

$$= \frac{i}{2}\bar{v}_{ijkl}\left(U_{l\alpha}[\chi^{11},f]_{\alpha\beta}V^\dagger_{\beta k} + U_{l\alpha}\left(\chi^{12} - \left\{\chi^{12},f\right\}\right)_{\alpha\beta}U^T_{\beta k}\right. \tag{B.43}$$

$$\left. -V^*_{l\alpha}\left(\chi^{21} - \left\{\chi^{21},f\right\}\right)_{\alpha\beta}V^\dagger_{\beta k} - V^*_{l\alpha}[\chi^{22},f]_{\alpha\beta}U^T_{\beta k}\right) \tag{B.44}$$

To clean up the presentation a bit, let us introduce the following:

$$J^{11}_{ij\alpha\beta} = i\bar{v}_{ikjl}U_{l\alpha}U^{\dagger}_{\beta k} \qquad J^{22}_{ij\alpha\beta} = -i\bar{v}_{ikjl}V^{*}_{l\alpha}V^{T}_{\beta k} \tag{B.45}$$

$$K^{12}_{ij\alpha\beta} = i\bar{v}_{ikjl}U_{l\alpha}V^{T}_{\beta k} \qquad K^{21}_{ij\alpha\beta} = -i\bar{v}_{ikjl}V^{*}_{l\alpha}U^{\dagger}_{\beta k} \tag{B.46}$$

$$L^{12}_{ij\alpha\beta} = i\bar{v}_{ijkl}U_{l\alpha}U^{T}_{\beta k} \qquad L^{21}_{ij\alpha\beta} = -i\bar{v}_{ijkl}V^{*}_{l\alpha}V^{\dagger}_{\beta k} \tag{B.47}$$

$$M^{11}_{ij\alpha\beta} = i\bar{v}_{ijkl}U_{l\alpha}V^{\dagger}_{\beta k} \qquad M^{22}_{ij\alpha\beta} = -i\bar{v}_{ijkl}V^{*}_{l\alpha}U^{T}_{\beta k} \tag{B.48}$$

Then the fields simplify to

$$\Gamma_{(1),ij} = J^{11}_{ij\alpha\beta}[\chi^{11}, f]_{\alpha\beta} + K^{12}_{ij\alpha\beta}\left(\chi^{12} - \left\{\chi^{12}, f\right\}\right)_{\alpha\beta} + K^{12}_{ij\alpha\beta}\left(\chi^{21} - \left\{\chi^{21}, f\right\}\right)_{\alpha\beta} + J^{22}_{ij\alpha\beta}[\chi^{22}, f]_{\alpha\beta} \tag{B.49}$$

$$2\Delta_{(1),ij} = M^{11}_{ij\alpha\beta}[\chi^{11}, f]_{\alpha\beta} + L^{12}_{ij\alpha\beta}\left(\chi^{12} - \left\{\chi^{12}, f\right\}\right)_{\alpha\beta} + L^{12}_{ij\alpha\beta}\left(\chi^{21} - \left\{\chi^{21}, f\right\}\right)_{\alpha\beta} + M^{22}_{ij\alpha\beta}[\chi^{22}, f]_{\alpha\beta} \tag{B.50}$$

Now we can transform the fields back into the quasiparticle basis:

$$\mathcal{H}_1 = \begin{pmatrix} U^{\dagger} & V^{\dagger} \\ V^{T} & U^{T} \end{pmatrix} \begin{pmatrix} \Gamma_1 & \Delta_1 \\ -\Delta_1^{*} & -\Gamma_1^{*} \end{pmatrix} \begin{pmatrix} U & V^{*} \\ V & U^{*} \end{pmatrix} \tag{B.51}$$

$$= \begin{pmatrix} U^{\dagger}\Gamma_1 U + U^{\dagger}\Delta_1 V - V^{\dagger}\Delta_1^{*}U - V^{\dagger}\Gamma_1^{*}V & U^{\dagger}\Gamma_1 V^{*} + U^{\dagger}\Delta_1 U^{*} - V^{\dagger}\Delta_1^{*}V^{*} - V^{\dagger}\Gamma_1^{*}U^{*} \\ V^{T}\Gamma_1 U + V^{T}\Delta_1 V - U^{T}\Delta_1^{*}U - U^{T}\Gamma_1^{*}V & V^{T}\Gamma_1 V^{*} + V^{T}\Delta_1 U^{*} - U^{T}\Delta_1^{*}V^{*} - U^{T}\Gamma_1^{*}U^{*} \end{pmatrix} \tag{B.52}$$

Assuming further that the full matrix χ is Hermitian, then $\chi^{11*} = \chi^{11}$, $\chi^{22*} = \chi^{22}$, and

$\chi^{12*} = \chi^{21}$. This leads in turn to

$$[\chi^{11}, f]^* = -[\chi^{11}, f] \tag{B.53}$$

$$[\chi^{22}, f]^* = -[\chi^{22}, f] \tag{B.54}$$

$$\left(\chi^{12} - \left\{\chi^{12}, f\right\}\right)^* = \left(\chi^{21} - \left\{\chi^{21}, f\right\}\right) \tag{B.55}$$

$$\left(\chi^{21} - \left\{\chi^{21}, f\right\}\right)^* = \left(\chi^{12} - \left\{\chi^{12}, f\right\}\right) \tag{B.56}$$

The whole thing written out is

$$\mathcal{H}^{11}_{(1),ab} = \left(U^\dagger_{ai}U_{jb}J^{11}_{ij\alpha\beta} + U^\dagger_{ai}V_{jb}\frac{M^{11}_{ij\alpha\beta}}{2} + V^\dagger_{ai}U_{jb}\frac{M^{11*}_{ij\alpha\beta}}{2} + V^\dagger_{ai}V_{jb}J^{11*}_{ij\alpha\beta}\right)(f_\beta - f_\alpha)\chi^{11}_{\alpha\beta} \tag{B.57}$$

$$+ \left(U^\dagger_{ai}U_{jb}J^{22}_{ij\alpha\beta} + U^\dagger_{ai}V_{jb}\frac{M^{22}_{ij\alpha\beta}}{2} + V^\dagger_{ai}U_{jb}\frac{M^{22*}_{ij\alpha\beta}}{2} + V^\dagger_{ai}V_{jb}J^{22*}_{ij\alpha\beta}\right)(f_\beta - f_\alpha)\chi^{22}_{\alpha\beta} \tag{B.58}$$

$$+ \left(U^\dagger_{ai}U_{jb}K^{12}_{ij\alpha\beta} + U^\dagger_{ai}V_{jb}\frac{L^{12}_{ij\alpha\beta}}{2} - V^\dagger_{ai}U_{jb}\frac{L^{21*}_{ij\alpha\beta}}{2} + V^\dagger_{ai}V_{jb}K^{21*}_{ij\alpha\beta}\right)\left(1 - f_\alpha - f_\beta\right)\chi^{12}_{\alpha\beta} \tag{B.59}$$

$$+ \left(U^\dagger_{ai}U_{jb}K^{21}_{ij\alpha\beta} + U^\dagger_{ai}V_{jb}\frac{L^{21}_{ij\alpha\beta}}{2} - V^\dagger_{ai}U_{jb}\frac{L^{12*}_{ij\alpha\beta}}{2} + V^\dagger_{ai}V_{jb}K^{12*}_{ij\alpha\beta}\right)\left(1 - f_\alpha - f_\beta\right)\chi^{21}_{\alpha\beta} \tag{B.60}$$

$$\mathcal{H}^{12}_{(1),ab} = \left(U^{\dagger}_{ai} V^{*}_{jb} J^{11}_{ij\alpha\beta} + U^{\dagger}_{ai} U^{*}_{jb} \frac{M^{11}_{ij\alpha\beta}}{2} + V^{\dagger}_{ai} V^{*}_{jb} \frac{M^{11*}_{ij\alpha\beta}}{2} + V^{\dagger}_{ai} U^{*}_{jb} J^{11*}_{ij\alpha\beta} \right) (f_\beta - f_\alpha) \chi^{11}_{\alpha\beta} \tag{B.61}$$

$$+ \left(U^{\dagger}_{ai} V^{*}_{jb} J^{22}_{ij\alpha\beta} + U^{\dagger}_{ai} U^{*}_{jb} \frac{M^{22}_{ij\alpha\beta}}{2} + V^{\dagger}_{ai} V^{*}_{jb} \frac{M^{22*}_{ij\alpha\beta}}{2} + V^{\dagger}_{ai} U^{*}_{jb} J^{22*}_{ij\alpha\beta} \right) (f_\beta - f_\alpha) \chi^{22}_{\alpha\beta} \tag{B.62}$$

$$+ \left(U^{\dagger}_{ai} V^{*}_{jb} K^{12}_{ij\alpha\beta} + U^{\dagger}_{ai} U^{*}_{jb} \frac{L^{12}_{ij\alpha\beta}}{2} - V^{\dagger}_{ai} V^{*}_{jb} \frac{L^{21*}_{ij\alpha\beta}}{2} + V^{\dagger}_{ai} U^{*}_{jb} K^{21*}_{ij\alpha\beta} \right) \left(1 - f_\alpha - f_\beta\right) \chi^{12}_{\alpha\beta} \tag{B.63}$$

$$+ \left(U^{\dagger}_{ai} V^{*}_{jb} K^{21}_{ij\alpha\beta} + U^{\dagger}_{ai} U^{*}_{jb} \frac{L^{21}_{ij\alpha\beta}}{2} - V^{\dagger}_{ai} V^{*}_{jb} \frac{L^{12*}_{ij\alpha\beta}}{2} + V^{\dagger}_{ai} U^{*}_{jb} K^{12*}_{ij\alpha\beta} \right) \left(1 - f_\alpha - f_\beta\right) \chi^{21}_{\alpha\beta} \tag{B.64}$$

$$\mathcal{H}^{21}_{(1),ab} = \left(V^{T}_{ai} U_{jb} J^{11}_{ij\alpha\beta} + V^{T}_{ai} V_{jb} \frac{M^{11}_{ij\alpha\beta}}{2} + U^{T}_{ai} U_{jb} \frac{M^{11*}_{ij\alpha\beta}}{2} + U^{T}_{ai} V_{jb} J^{11*}_{ij\alpha\beta} \right) (f_\beta - f_\alpha) \chi^{11}_{\alpha\beta} \tag{B.65}$$

$$+ \left(V^{T}_{ai} U_{jb} J^{22}_{ij\alpha\beta} + V^{T}_{ai} V_{jb} \frac{M^{22}_{ij\alpha\beta}}{2} + U^{T}_{ai} U_{jb} \frac{M^{22*}_{ij\alpha\beta}}{2} + U^{T}_{ai} V_{jb} J^{22*}_{ij\alpha\beta} \right) (f_\beta - f_\alpha) \chi^{22}_{\alpha\beta} \tag{B.66}$$

$$+ \left(V^{T}_{ai} U_{jb} K^{12}_{ij\alpha\beta} + V^{T}_{ai} V_{jb} \frac{L^{12}_{ij\alpha\beta}}{2} - U^{T}_{ai} U_{jb} \frac{L^{21*}_{ij\alpha\beta}}{2} + U^{T}_{ai} V_{jb} K^{21*}_{ij\alpha\beta} \right) \left(1 - f_\alpha - f_\beta\right) \chi^{12}_{\alpha\beta} \tag{B.67}$$

$$+ \left(V^{T}_{ai} U_{jb} K^{21}_{ij\alpha\beta} + V^{T}_{ai} V_{jb} \frac{L^{21}_{ij\alpha\beta}}{2} - U^{T}_{ai} U_{jb} \frac{L^{12*}_{ij\alpha\beta}}{2} + U^{T}_{ai} V_{jb} K^{12*}_{ij\alpha\beta} \right) \left(1 - f_\alpha - f_\beta\right) \chi^{21}_{\alpha\beta} \tag{B.68}$$

$$\mathcal{H}^{22}_{(1),ab} = \left(V^T_{ai} V^*_{jb} J^{11}_{ij\alpha\beta} + V^T_{ai} U^*_{jb} \frac{M^{11}_{ij\alpha\beta}}{2} + U^T_{ai} V^*_{jb} \frac{M^{11*}_{ij\alpha\beta}}{2} + U^T_{ai} U^*_{jb} J^{11*}_{ij\alpha\beta} \right) (f_\beta - f_\alpha) \chi^{11}_{\alpha\beta} \tag{B.69}$$

$$+ \left(V^T_{ai} V^*_{jb} J^{22}_{ij\alpha\beta} + V^T_{ai} U^*_{jb} \frac{M^{22}_{ij\alpha\beta}}{2} + U^T_{ai} V^*_{jb} \frac{M^{22*}_{ij\alpha\beta}}{2} + U^T_{ai} U^*_{jb} J^{22*}_{ij\alpha\beta} \right) (f_\beta - f_\alpha) \chi^{22}_{\alpha\beta} \tag{B.70}$$

$$+ \left(V^T_{ai} V^*_{jb} K^{12}_{ij\alpha\beta} + V^T_{ai} U^*_{jb} \frac{L^{12}_{ij\alpha\beta}}{2} - U^T_{ai} V^*_{jb} \frac{L^{21*}_{ij\alpha\beta}}{2} + U^T_{ai} U^*_{jb} K^{21*}_{ij\alpha\beta} \right) \left(1 - f_\alpha - f_\beta\right) \chi^{12}_{\alpha\beta} \tag{B.71}$$

$$+ \left(V^T_{ai} V^*_{jb} K^{21}_{ij\alpha\beta} + V^T_{ai} U^*_{jb} \frac{L^{21}_{ij\alpha\beta}}{2} - U^T_{ai} V^*_{jb} \frac{L^{12*}_{ij\alpha\beta}}{2} + U^T_{ai} U^*_{jb} K^{12*}_{ij\alpha\beta} \right) \left(1 - f_\alpha - f_\beta\right) \chi^{21}_{\alpha\beta} \tag{B.72}$$

Looking back to B.35, we see that we can write it in the same form as B.34:

$$\begin{aligned}
\frac{1}{2}\mathrm{Tr}\left(\mathcal{H}_1 \mathcal{R}_1\right) = & \bar{\mathcal{M}}''^{11,11}_{\alpha\beta ab} \chi^{11}_{\alpha\beta} \chi^{11}_{ba} + \bar{\mathcal{M}}''^{12,11}_{\alpha\beta ab} \chi^{12}_{\alpha\beta} \chi^{11}_{ba} + \bar{\mathcal{M}}''^{21,11}_{\alpha\beta ab} \chi^{21}_{\alpha\beta} \chi^{11}_{ba} + \bar{\mathcal{M}}''^{22,11}_{\alpha\beta ab} \chi^{22}_{\alpha\beta} \chi^{11}_{ba} \\
& \bar{\mathcal{M}}''^{11,12}_{\alpha\beta ab} \chi^{11}_{\alpha\beta} \chi^{12}_{ba} + \bar{\mathcal{M}}''^{12,12}_{\alpha\beta ab} \chi^{12}_{\alpha\beta} \chi^{12}_{ba} + \bar{\mathcal{M}}''^{21,12}_{\alpha\beta ab} \chi^{21}_{\alpha\beta} \chi^{12}_{ba} + \bar{\mathcal{M}}''^{22,12}_{\alpha\beta ab} \chi^{22}_{\alpha\beta} \chi^{12}_{ba} \\
& \bar{\mathcal{M}}''^{11,21}_{\alpha\beta ab} \chi^{11}_{\alpha\beta} \chi^{21}_{ba} + \bar{\mathcal{M}}''^{12,21}_{\alpha\beta ab} \chi^{12}_{\alpha\beta} \chi^{21}_{ba} + \bar{\mathcal{M}}''^{21,21}_{\alpha\beta ab} \chi^{21}_{\alpha\beta} \chi^{21}_{ba} + \bar{\mathcal{M}}''^{22,21}_{\alpha\beta ab} \chi^{22}_{\alpha\beta} \chi^{21}_{ba} \\
& \bar{\mathcal{M}}''^{11,22}_{\alpha\beta ab} \chi^{11}_{\alpha\beta} \chi^{22}_{ba} + \bar{\mathcal{M}}''^{12,22}_{\alpha\beta ab} \chi^{12}_{\alpha\beta} \chi^{22}_{ba} + \bar{\mathcal{M}}''^{21,22}_{\alpha\beta ab} \chi^{21}_{\alpha\beta} \chi^{22}_{ba} + \bar{\mathcal{M}}''^{22,22}_{\alpha\beta ab} \chi^{22}_{\alpha\beta} \chi^{22}_{ba}
\end{aligned} \tag{B.73}$$

B.3.4 The Inertia Tensor

B.3.4.1 The total kinetic energy

Expressions B.34 and B.73 can be combined into one single expression involving the vector-like object χ and the matrix-like object $\bar{\mathcal{M}} = 2(\bar{\mathcal{M}}' + \bar{\mathcal{M}}'')$

$$E_{kin} = \frac{1}{2}\chi^{\dagger}\bar{\mathcal{M}}\chi \tag{B.74}$$

$$\chi_{\alpha\beta} \equiv \begin{pmatrix} \chi^{11}_{\alpha\beta} \\ \chi^{12}_{\alpha\beta} \\ \chi^{21}_{\alpha\beta} \\ \chi^{22}_{\alpha\beta} \end{pmatrix}, \qquad \chi^{\dagger}_{ab} = \begin{pmatrix} \chi^{11*}_{ab} \chi^{12*}_{ab} \chi^{21*}_{ab} \chi^{22*}_{ab} \end{pmatrix} \tag{B.75}$$

$\bar{\mathcal{M}}$ is given by column in Table B.1.

Now we have an expression for the energy in terms of an inertia tensor $\bar{\mathcal{M}}$ and the expansion parameter χ. We already know that χ is related to time-dependent changes in the density $\dot{\mathcal{R}}_0$; now let us further try to relate χ to changes in the collective shape multipole moments of the nucleus $\dot{q}$.

Sanity Check: As in the case of the ATDHFB equations from section B.3.2, in the $T = f = 0$ case, the ^{11} and ^{22} terms vanish completely in the lines leading up to B.34 and B.73 and we are left with familiar [zero-temperature] ATDHFB expressions. In essence, the rank of the problem reduces from dealing with a 4x4 matrix to dealing with a 2x2 matrix.

Table B.1: The full FT-ATDHFB matrix, listed by column

$$\bar{\mathcal{M}}_{:1} = \frac{1}{2}\begin{pmatrix} (E_b - E_a)(f_a - f_b)\delta_{a\alpha}\delta_{b\beta} - (f_a - f_b)\left[\bar{v}_{ikjl}\left(U^\dagger_{ai}U_{jb}U_{l\alpha}U^\dagger_{\beta k} - V^\dagger_{ai}V_{jb}U^*_{l\alpha}U^T_{\beta k}\right) + \frac{\bar{v}_{ijkl}}{2}\left(U^\dagger_{ai}V_{jb}U_{l\alpha}V^\dagger_{\beta k} - V^\dagger_{ai}U_{jb}U^*_{l\alpha}V^T_{\beta k}\right)\right](f_\beta - f_\alpha \\ (1 - f_a - f_b)\left[\bar{v}_{ikjl}\left(U^\dagger_{ai}V^*_{jb}U_{l\alpha}U^\dagger_{\beta k} - V^\dagger_{ai}U^*_{jb}U^*_{l\alpha}U^T_{\beta k}\right) + \frac{\bar{v}_{ijkl}}{2}\left(U^\dagger_{ai}U^*_{jb}U_{l\alpha}V^\dagger_{\beta k} - V^\dagger_{ai}V^*_{jb}U^*_{l\alpha}V^T_{\beta k}\right)\right](f_\beta - f_\alpha) \\ -(1 - f_a - f_b)\left[\bar{v}_{ikjl}\left(V^T_{ai}U_{jb}U_{l\alpha}U^\dagger_{\beta k} - U^T_{ai}V_{jb}U^*_{l\alpha}U^T_{\beta k}\right) + \frac{\bar{v}_{ijkl}}{2}\left(V^T_{ai}V_{jb}U_{l\alpha}V^\dagger_{\beta k} - U^T_{ai}U_{jb}U^*_{l\alpha}V^T_{\beta k}\right)\right](f_\beta - f_\alpha) \\ (f_a - f_b)\left[\bar{v}_{ikjl}\left(V^T_{ai}V^*_{jb}U_{l\alpha}U^\dagger_{\beta k} - U^T_{ai}U^*_{jb}U^*_{l\alpha}U^T_{\beta k}\right) + \frac{\bar{v}_{ijkl}}{2}\left(V^T_{ai}U^*_{jb}U_{l\alpha}V^\dagger_{\beta k} - U^T_{ai}V^*_{jb}U^*_{l\alpha}V^T_{\beta k}\right)\right](f_\beta - f_\alpha) \end{pmatrix} \tag{B.76}$$

$$\bar{\mathcal{M}}_{:2} = \frac{1}{2}\begin{pmatrix} -(f_a - f_b)\left[\bar{v}_{ikjl}\left(U^\dagger_{ai}U_{jb}U_{l\alpha}V^T_{\beta k} + V^\dagger_{ai}V_{jb}V_{l\alpha}U^T_{\beta k}\right) + \frac{\bar{v}_{ijkl}}{2}\left(U^\dagger_{ai}V_{jb}U_{l\alpha}U^T_{\beta k} - V^\dagger_{ai}U_{jb}V_{l\alpha}V^T_{\beta k}\right)\right](1 - f_\alpha - f_\beta) \\ (E_a + E_b)(1 - f_a - f_b)\delta_{a\alpha}\delta_{b\beta} + (1 - f_a - f_b)\left[\bar{v}_{ikjl}\left(U^\dagger_{ai}V^*_{jb}U_{l\alpha}V^T_{\beta k} + V^\dagger_{ai}U^*_{jb}V_{l\alpha}U^T_{\beta k}\right) + \frac{\bar{v}_{ijkl}}{2}\left(U^\dagger_{ai}U^*_{jb}U_{l\alpha}U^T_{\beta k} - V^\dagger_{ai}V^*_{jb}V_{l\alpha}V^T_{\beta k}\right)\right](1 \\ -(1 - f_a - f_b)\left[\bar{v}_{ikjl}\left(V^T_{ai}U_{jb}U_{l\alpha}V^T_{\beta k} + U^T_{ai}V_{jb}V_{l\alpha}U^T_{\beta k}\right) + \frac{\bar{v}_{ijkl}}{2}\left(V^T_{ai}V_{jb}U_{l\alpha}U^T_{\beta k} - U^T_{ai}U_{jb}V_{l\alpha}V^T_{\beta k}\right)\right](1 - f_\alpha - f_\beta) \\ (f_a - f_b)\left[\bar{v}_{ikjl}\left(V^T_{ai}V^*_{jb}U_{l\alpha}V^T_{\beta k} + U^T_{ai}U^*_{jb}V_{l\alpha}U^T_{\beta k}\right) + \frac{\bar{v}_{ijkl}}{2}\left(V^T_{ai}U^*_{jb}U_{l\alpha}U^T_{\beta k} - U^T_{ai}V^*_{jb}V_{l\alpha}V^T_{\beta k}\right)\right](1 - f_\alpha - f_\beta) \end{pmatrix} \tag{B.77}$$

$$\bar{\mathcal{M}}_{:3} = \frac{1}{2}\begin{pmatrix} (f_a - f_b)\left[\bar{v}_{ikjl}\left(U^\dagger_{ai}U_{jb}V^*_{l\alpha}U^\dagger_{\beta k} + V^\dagger_{ai}V_{jb}U^*_{l\alpha}V^\dagger_{\beta k}\right) + \frac{\bar{v}_{ijkl}}{2}\left(U^\dagger_{ai}V_{jb}V^*_{l\alpha}V^\dagger_{\beta k} - V^\dagger_{ai}U_{jb}U^*_{l\alpha}U^\dagger_{\beta k}\right)\right](1 - f_\alpha - f_\beta) \\ -(1 - f_a - f_b)\left[\bar{v}_{ikjl}\left(U^\dagger_{ai}V^*_{jb}V^*_{l\alpha}U^\dagger_{\beta k} + V^\dagger_{ai}U^*_{jb}U^*_{l\alpha}V^\dagger_{\beta k}\right) + \frac{\bar{v}_{ijkl}}{2}\left(U^\dagger_{ai}U^*_{jb}V^*_{l\alpha}V^\dagger_{\beta k} - V^\dagger_{ai}V^*_{jb}U^*_{l\alpha}U^\dagger_{\beta k}\right)\right](1 - f_\alpha - f_\beta) \\ (E_a + E_b)(1 - f_a - f_b)\delta_{a\alpha}\delta_{b\beta} + (1 - f_a - f_b)\left[\bar{v}_{ikjl}\left(V^T_{ai}U_{jb}V^*_{l\alpha}U^\dagger_{\beta k} + U^T_{ai}V_{jb}U^*_{l\alpha}V^\dagger_{\beta k}\right) + \frac{\bar{v}_{ijkl}}{2}\left(V^T_{ai}V_{jb}V^*_{l\alpha}V^\dagger_{\beta k} - U^T_{ai}U_{jb}U^*_{l\alpha}U^\dagger_{\beta k}\right)\right] \\ -(f_a - f_b)\left[\bar{v}_{ikjl}\left(V^T_{ai}V^*_{jb}V^*_{l\alpha}U^\dagger_{\beta k} + U^T_{ai}U^*_{jb}U^*_{l\alpha}V^\dagger_{\beta k}\right) + \frac{\bar{v}_{ijkl}}{2}\left(V^T_{ai}U^*_{jb}V^*_{l\alpha}V^\dagger_{\beta k} - U^T_{ai}V^*_{jb}U^*_{l\alpha}U^\dagger_{\beta k}\right)\right](1 - f_\alpha - f_\beta) \end{pmatrix} \tag{B.78}$$

$$\bar{\mathcal{M}}_{:4} = \frac{1}{2}\begin{pmatrix} (f_a - f_b)\left[\bar{v}_{ikjl}\left(U^\dagger_{ai}U_{jb}V^*_{l\alpha}V^T_{\beta k} - V^\dagger_{ai}V_{jb}V_{l\alpha}V^\dagger_{\beta k}\right) + \frac{\bar{v}_{ijkl}}{2}\left(U^\dagger_{ai}V_{jb}V^*_{l\alpha}U^T_{\beta k} - V^\dagger_{ai}U_{jb}V_{l\alpha}U^\dagger_{\beta k}\right) +\right](f_\beta - f_\alpha) \\ -(1 - f_a - f_b)\left[\bar{v}_{ikjl}\left(U^\dagger_{ai}V^*_{jb}V^*_{l\alpha}V^T_{\beta k} - V^\dagger_{ai}U^*_{jb}V_{l\alpha}V^\dagger_{\beta k}\right) + \frac{\bar{v}_{ijkl}}{2}\left(U^\dagger_{ai}U^*_{jb}V^*_{l\alpha}U^T_{\beta k} - V^\dagger_{ai}V^*_{jb}V_{l\alpha}U^\dagger_{\beta k}\right)\right](f_\beta - f_\alpha) \\ (1 - f_a - f_b)\left[\bar{v}_{ikjl}\left(V^T_{ai}U_{jb}V^*_{l\alpha}V^T_{\beta k} - U^T_{ai}V_{jb}V_{l\alpha}V^\dagger_{\beta k}\right) + \frac{\bar{v}_{ijkl}}{2}\left(V^T_{ai}V_{jb}V^*_{l\alpha}U^T_{\beta k} - U^T_{ai}U_{jb}V_{l\alpha}U^\dagger_{\beta k}\right)\right](f_\beta - f_\alpha) \\ (E_b - E_a)(f_a - f_b)\delta_{a\alpha}\delta_{b\beta} - (f_a - f_b)\left[\bar{v}_{ikjl}\left(V^T_{ai}V^*_{jb}V^*_{l\alpha}V^T_{\beta k} - U^T_{ai}U^*_{jb}V_{l\alpha}V^\dagger_{\beta k}\right) + \frac{\bar{v}_{ijkl}}{2}\left(V^T_{ai}U^*_{jb}V^*_{l\alpha}U^T_{\beta k} - U^T_{ai}V^*_{jb}V_{l\alpha}U^\dagger_{\beta k}\right)\right](f_\beta - f_\alpha \end{pmatrix} \tag{B.79}$$

B.3.4.2 Cranking Approximation

We already introduced the cranking approximation briefly in section B.3.2 to simplify the relation between χ and $\dot{\mathcal{R}}_0$ when we assumed that changes in the density will have approximately no effect on the mean field ($\mathcal{H}_1 \approx 0$). We can apply this to the energy expression, and then the inertia tensor is much simpler:

$$\bar{\mathcal{M}} = \frac{1}{4}\begin{pmatrix} (E_b - E_a)(f_a - f_b) & 0 & 0 & 0 \\ 0 & (E_a + E_b)(1 - f_a - f_b) & 0 & 0 \\ 0 & 0 & (E_a + E_b)(1 - f_a - f_b) & 0 \\ 0 & 0 & 0 & (E_b - E_a)(f_a - f_b) \end{pmatrix} \tag{B.80}$$

B.3.4.3 The Collective Shape Space

Suppose there is a set of collective variables $(q_1, q_2, \ldots, q_n)$ which describe changes in the density $\mathcal{R}_0(t)$ at all times t. Then

$$\dot{\mathcal{R}}_0 = \sum_{\mu=1}^{n} \dot{q_\mu} \frac{\partial \mathcal{R}_0}{\partial q_\mu} \tag{B.81}$$

Relating this back to χ using equations B.20 (we'll just stick with the cranking approximation here) gives

$$\chi_{ab}^{11} = \sum_{\mu=1}^{n} \frac{\hbar \dot{q_\mu}}{(E_a - E_b)(f_b - f_a)} \frac{\partial \mathcal{R}_{(0),ab}^{11}}{\partial q_\mu} \tag{B.82}$$

$$\chi_{ab}^{12} = \sum_{\mu=1}^{n} \frac{\hbar \dot{q_\mu}}{(E_a + E_b)(1 - f_a - f_b)} \frac{\partial \mathcal{R}_{(0),ab}^{12}}{\partial q_\mu} \tag{B.83}$$

$$\chi_{ab}^{21} = \sum_{\mu=1}^{n} \frac{\hbar \dot{q_\mu}}{(E_a + E_b)(1 - f_a - f_b)} \frac{\partial \mathcal{R}_{(0),ab}^{21}}{\partial q_\mu} \tag{B.84}$$

$$\chi_{ab}^{22} = \sum_{\mu=1}^{n} \frac{\hbar \dot{q_\mu}}{(E_a - E_b)(f_b - f_a)} \frac{\partial \mathcal{R}_{(0),ab}^{22}}{\partial q_\mu} \tag{B.85}$$

$$\tag{B.86}$$

Of course, we should be careful here if the temperature is allowed to approach zero. In that case, then from equation B.20 we see that $\dot{\mathcal{R}}^{11} = \dot{\mathcal{R}}^{22} = 0$. We should not have any χ^{11} or χ^{22} terms in the zero temperature case. The final form of the inertia tensor will also be affected. Likewise we should be careful not to divide by zero in the case of $E_a = E_b$ as mentioned earlier at the end of section B.3.2.

If we take this now and plug it into our energy expression B.74 using the cranked inertia tensor B.80, the result is the following:

$$E_{kin} \approx \frac{1}{2} \sum_{\mu\nu} \dot{q}_\mu \dot{q}_\nu \mathsf{M}_{\mu\nu} \tag{B.87}$$

where

$$\mathsf{M}_{\mu\nu} = \frac{\hbar^2}{2}\left[\frac{1}{(E_a - E_b)(f_b - f_a)}\left(\frac{\partial \mathcal{R}^{11}_{(0),ab}}{\partial q_\mu}\frac{\partial \mathcal{R}^{11}_{(0),ba}}{\partial q_\nu} + \frac{\partial \mathcal{R}^{22}_{(0),ab}}{\partial q_\mu}\frac{\partial \mathcal{R}^{22}_{(0),ba}}{\partial q_\mu}\right) + \frac{1}{(E_a + E_b)(1 - f_a - f_b)}\left(\frac{\partial \mathcal{R}^{21}_{(0),ab}}{\partial q_\mu}\frac{\partial \mathcal{R}^{12}_{(0),ba}}{\partial q_\nu} + \frac{\partial \mathcal{R}^{12}_{(0),ab}}{\partial q_\mu}\frac{\partial \mathcal{R}^{21}_{(0),ba}}{\partial q_\mu}\right)\right] \tag{B.88}$$

In the zero temperature case, the first piece (involving $\mathcal{R}^{11}$ and $\mathcal{R}^{22}$) should be replaced with zero.

B.4 Numerical implementation

Numerical implementations of the FT-ATDHFB inertia may encounter some challenges. First, as discussed in Section 3.2we know there is an ideal range of values δq to use when computing derivatives of $\mathcal{R}$ using finite differences. Too large, and the derivative is artifically-smoothed out; too small, and densities of adjacent points can become indistinguishable (dependent on the HFB convergence parameter). Additionally, there may be problems when dealing with small, non-zero temperatures (or, more generally, when $f_b - f_a$ is small).

We might consider introducing a cutoff on the difference $f_b - f_a$. If we make our cutoff too tight, we start cutting off physics (the tail of the Fermi distribution). If we leave our cutoff too small, we start dividing by numbers that are smaller than the noise in the density matrix which will lead to the inertia blowing up.

As an example, suppose we take a value $\delta q = 10^{-3}$ and set our HFB convergence parameter to 10^{-7}. Roughly-speaking, then, we would expect that we can set a cutoff for $f_b - f_a$ of something around 10^{-4} or so and still obtain reasonable results.

This was done for a ^{240}Pu calculation with a few different cutoff values. First the exact T=0 inertia was computed. Then the inertia was computed again using the same densities which had been computed at T=0, but introducing a fake temperature T=0.05 to calculate the inertia. The results, shown in the following table, indicate the presence of an ideal cutoff parameter that is in the neighborhood of our prediction:

Convergence	10^{-7}	
δq	10^{-3}	
Actual T=0 inertia:	1.585632E-02	
Cutoff	**Inertia**	**% error**
10^{-4}	1.585205E-02	-2.692933E-04
10^{-5}	1.585622E-02	-6.306634E-06
10^{-6}	1.585697E-02	4.099312E-05
10^{-7}	1.587771E-02	1.348989E-03
10^{-8}	1.612200E-02	1.675546E-02

Appendix C

List of my contributions

- **Observation of the competing fission modes in ^{178}Pt**
  - *Phys. Lett. B 790, 583-588 (2019)*
  - Performed PES calculations
  - Created graphics for Figure 3
  - Suggested several revisions to the text of the article
- **Colloquium: Superheavy elements: Oganesson and beyond**
  - *Rev. Mod. Phys. 91, 011001 (2019)*
  - Generated Figure 12
  - Helped write Section VI: Fission
  - Suggested comments and revisions to the text
- **Cluster radioactivity of ^{294}Og**
  - *???*
  - Lead author on paper/wrote first draft
  - Did all UNEDF1$_{\mathrm{HFB}}$ calculations and SkM* Langevin calculations
  - Generated all figures

- **Microscopic Calculation of Fission Mass Distributions at Increasing Excitation Energies**
  - *CNR2018 Proceedings...*
  - Helped derive [one of the equations]
  - Contributed to discussion of ???
- **Fission Tools**
  - *Suite of codes which extend the functionality of HFODD, HFBTHO, and other DFT solvers to the problem of nuclear fission.*
  - `https://gitlab.com/zachmath/fission_tools`
  - Maintainer, 47 commits
  - Converted old codes from Fortran77 to Fortran90
  - Implemented shared memory (OpenMP) and distributed memory (MPI) parallelism
  - Improved documentation, flexibility, and user-friendliness
  - Created several Python-based utilities for plotting and file handling
  - Increased functionality, such as by increasing from 2D to 3D or 4D
- **PES Tools**
  - *Python framework for handling potential energy surfaces as XML files*
  - `https://gitlab.com/schuncknf/pes_tools`
  - Developer, 24 commits

  - Added a `point` class with various methods to use on a single point of a PES
  - Interface to `fission_tools`
  - Various updates bugfixes

- **DFTNESS**
  - *DFTNESS (Density Functional Theory for Nuclei at Extreme ScaleS) is a computational framework to solve the equation of nuclear density functional theory. It is based on the two solvers HFBTHO and HFODD.*
  - `https://gitlab.com/schuncknf/dftness`
  - https://gitlab.com/schuncknf/dftness
  - Developer, 60 commits
  - OpenMP parallelization of subroutine `QMULCM`
  - Various updates and bugfixes
  - Most of these commits were related to `fission_tools`, before that was all moved to a separate repository

BIBLIOGRAPHY

[1] O. Hahn and F. Strassmann, Naturwissenschaften **27**, 11 (1939).

[2] L. Meitner and O. R. Frisch, Nature **143**, 239 (1939).

[3] N. Bohr, Nature **143**, 330 (1939).

[4] G. Flerov and K. Petrjak, Phys. Rev. **58**, 89 (1940).

[5] N. Schunck and L. M. Robledo, Reports Prog. Phys. **79**, 116301 (2016).

[6] C. F. v. Weizs\"acker, Zeitschrift f\"ur Phys. **96**, 431 (1935).

[7] N. Bohr and J. A. Wheeler, Phys. Rev. **56**, 426 (1939).

[8] V. Strutinsky, Nucl. Phys. A **95**, 420 (1967).

[9] V. Strutinsky, Nucl. Phys. A **122**, 1 (1968).

[10] M. Brack, J. Damgaard, A. S. Jensen, H. C. Pauli, V. M. Strutinsky, and C. Y. Wong, Rev. Mod. Phys. **44**, 320 (1972).

[11] J. Carlson, M. J. Savage, R. Gerber, K. Antypas, D. Bard, R. Coffey, E. Dart, S. Dosanjh, J. Hack, I. Monga, M. E. Papka, K. Riley, L. Rotman, T. Straatsma, J. Wells, H. Avakian, Y. Ayyad, S. A. Bass, D. Bazin, A. Boehnlein, G. Bollen, L. J. Broussard, A. Calder, S. Couch, A. Couture, M. Cromaz, W. Detmold, J. Detwiler, H. Duan, R. Edwards, J. Engel, C. Fryer, G. M. Fuller, S. Gandolfi, G. Gavalian, D. Georgobiani, R. Gupta, V. Gyurjyan, M. Hausmann, G. Heyes, W. R. Hix, M. Ito, G. Jansen, R. Jones, B. Joo, O. Kaczmarek, D. Kasen, M. Kostin, T. Kurth, J. Lauret, D. Lawrence, H.-W. Lin, M. Lin, P. Mantica, P. Maris, B. Messer, W. Mittig, S. Mosby, S. Mukherjee, H. A. Nam, P. Navratil, W. Nazarewicz, E. Ng, T. O'Donnell, K. Orginos, F. Pellemoine, P. Petreczky, S. C. Pieper, C. H. Pinkenburg, B. Plaster, R. J. Porter, M. Portillo, S. Pratt, M. L. Purschke, J. Qiang, S. Quaglioni, D. Richards, Y. Roblin, B. Schenke, R. Schiavilla, S. Schlichting, N. Schunck, P. Steinbrecher, M. Strickland, S. Syritsyn, B. Terzic, R. Varner, J. Vary, S. Wild, F. Winter, R. Zegers, H. Zhang, V. Ziegler, and M. Zingale, (2017), 10.2172/1369223.

[12] T. Baumann, M. Hausmann, B. Sherrill, and O. Tarasov, Nucl. Instruments Methods Phys. Res. Sect. B Beam Interact. with Mater. Atoms **376**, 33 (2016).

[13] G. Scamps and C. Simenel, (2018), arXiv:1804.03337 .

[14] G. Scamps, C. Simenel, and D. Lacroix, AIP Conf. Proc. **1681**, 040003 (2015).

[15] C. Simenel and A. S. Umar, Phys. Rev. C **89**, 031601 (2014).

[16] J. Grineviciute, P. Magierski, A. Bulgac, S. Jin, and I. Stetcu, Acta Phys. Pol. B **49**, 591 (2018).

[17] A. S. Umar, V. E. Oberacker, J. A. Maruhn, and P.-G. Reinhard, J. Phys. G Nucl. Part. Phys. **37**, 064037 (2010).

[18] G. Scamps, C. Simenel, and D. Lacroix, Phys. Rev. C **92**, 011602 (2015).

[19] A. Bulgac, S. Jin, K. Roche, N. Schunck, and I. Stetcu, (2018), arXiv:1806.00694 .

[20] R. Navarro Pérez, N. Schunck, A. Dyhdalo, R. J. Furnstahl, and S. K. Bogner, Phys. Rev. C **97**, 054304 (2018), arXiv:1801.08615 .

[21] M. Bender, P.-H. Heenen, and P.-G. Reinhard, Rev. Mod. Phys. **75**, 121 (2003), arXiv:9910025 [nucl-th] .

[22] J. Bartel, P. Quentin, M. Brack, C. Guet, and H.-B. Håkansson, Nucl. Phys. A **386**, 79 (1982).

[23] M. Kortelainen, J. McDonnell, W. Nazarewicz, P.-G. Reinhard, J. Sarich, N. Schunck, M. V. Stoitsov, and S. M. Wild, Phys. Rev. C **85**, 024304 (2012), arXiv:arXiv:1111.4344v2 .

[24] N. Schunck, J. D. McDonnell, J. Sarich, S. M. Wild, and D. Higdon, J. Phys. G Nucl. Part. Phys. **42**, 034024 (2015).

[25] P. Ring and P. Schuck, *The Nuclear Many-Body Problem*, edited by W. Beiglbock, M. Goldhaber, E. H. Lieb, and W. Thirring (Springer-Verlag, New York, 1980) p. 716.

[26] C. L. Zhang, B. Schuetrumpf, and W. Nazarewicz, Phys. Rev. C **94**, 064323 (2016), arXiv:arXiv:1607.00422v3 .

[27] J. Sadhukhan, C. Zhang, W. Nazarewicz, and N. Schunck, Phys. Rev. C **96**, 061301 (2017), arXiv:1711.10681 .

[28] J. Sadhukhan, W. Nazarewicz, and N. Schunck, Phys. Rev. C **93**, 011304 (2016), arXiv:1510.08003 .

[29] J. Sadhukhan, K. Mazurek, A. Baran, J. Dobaczewski, W. Nazarewicz, and J. A. Sheikh, Phys. Rev. C **88**, 064314 (2013), arXiv:1310.2003 .

[30] W. Younes and D. Gogny, *Fragment Yields Calculated in a Time-Dependent Microscopic Theory of Fission*, Tech. Rep. (Lawrence Livermore National Laboratory (LLNL), Livermore, CA (United States), 2012).

[31] A. Baran, J. A. Sheikh, J. Dobaczewski, W. Nazarewicz, and A. Staszczak, Phys. Rev. C **84**, 054321 (2011), arXiv:1007.3763 .

[32] S. A. Giuliani and L. M. Robledo, Phys. Lett. B **787**, 134 (2018).

[33] A. Baran, K. Pomorski, A. Lukasiak, and A. Sobiczewski, Nucl. Phys. A **361**, 83 (1981).

[34] A. Baran, Phys. Lett. B **76**, 8 (1978).

[35] K.-H. Schmidt and B. Jurado, Reports Prog. Phys. **81**, 106301 (2018), arXiv:1804.10421 .

[36] N. Schunck, J. Dobaczewski, W. Satuła, P. Baczyk, J. Dudek, Y. Gao, M. Konieczka, K. Sato, Y. Shi, X. Wang, and T. Werner, Comput. Phys. Commun. **216**, 145 (2017), arXiv:1612.05314 .

[37] R. N. Perez, N. Schunck, R.-D. Lasseri, C. Zhang, and J. Sarich, Comput. Phys. Commun. **220**, 363 (2017), arXiv:0406075 [nucl-th] .

[38] A. N. Andreyev, J. Elseviers, M. Huyse, P. Van Duppen, S. Antalic, A. Barzakh, N. Bree, T. E. Cocolios, V. F. Comas, J. Diriken, D. Fedorov, V. Fedosseev, S. Franchoo, J. A. Heredia, O. Ivanov, U. Köster, B. A. Marsh, K. Nishio, R. D. Page, N. Patronis, M. Seliverstov, I. Tsekhanovich, P. Van den Bergh, J. Van De Walle, M. Venhart, S. Vermote, M. Veselsky, C. Wagemans, T. Ichikawa, A. Iwamoto, P. Möller, and A. J. Sierk, Phys. Rev. Lett. **105**, 252502 (2010).

[39] V. Liberati, A. N. Andreyev, S. Antalic, A. Barzakh, T. E. Cocolios, J. Elseviers, D. Fedorov, V. N. Fedoseeev, M. Huyse, D. T. Joss, Z. Kalaninová, U. Köster, J. F. W. Lane, B. Marsh, D. Mengoni, P. Molkanov, K. Nishio, R. D. Page, N. Patronis, D. Pauwels, D. Radulov, M. Seliverstov, M. Sjödin, I. Tsekhanovich, P. Van den Bergh, P. Van Duppen, M. Venhart, and M. Veselský, Phys. Rev. C **88**, 044322 (2013).

[40] A. N. Andreyev, M. Huyse, and P. Van Duppen, Rev. Mod. Phys. **85**, 1541 (2013).

[41] J.-F. Martin, J. Taieb, A. Chatillon, G. Bélier, G. Boutoux, A. Ebran, T. Gorbinet, L. Grente, B. Laurent, E. Pellereau, H. Alvarez-Pol, L. Audouin, T. Aumann, Y. Ayyad, J. Benlliure, E. Casarejos, D. Cortina Gil, M. Caamaño, F. Farget, B. Fernández Domínguez, A. Heinz, B. Jurado, A. Kelić-Heil, N. Kurz, C. Nociforo, C. Paradela, S. Pietri, D. Ramos, J.-L. Rodríguez-Sànchez, C. Rodríguez-Tajes, D. Rossi, K.-H. Schmidt, H. Simon, L. Tassan-Got, J. Vargas, B. Voss, and H. Weick, Eur. Phys. J. A **51**, 174 (2015).

[42] A. N. Andreyev, K. Nishio, and K.-H. Schmidt, Reports Prog. Phys. **81**, 016301 (2018).

[43] J. Berger, M. Girod, and D. Gogny, Nucl. Phys. A **502**, 85 (1989).

[44] P. Möller, J. Randrup, and A. J. Sierk, Phys. Rev. C **85**, 024306 (2012).

[45] M. Warda, A. Staszczak, and W. Nazarewicz, Phys. Rev. C **86**, 024601 (2012), arXiv:arXiv:1205.5797v2 .

[46] J. D. McDonnell, W. Nazarewicz, J. A. Sheikh, A. Staszczak, and M. Warda, Phys. Rev. C **90**, 021302 (2014), arXiv:arXiv:1406.6955v1 .

[47] A. V. Karpov, V. I. Zagrebaev, Y. M. Palenzuela, and W. Greiner, , 1.

[48] M. Warda and J. L. Egido, Phys. Rev. C **86**, 014322 (2012), arXiv:1204.5867 .

[49] A. Sandulescu, D. Poenaru, and W. Greiner, Sov. J. Part. Nucl. **11**, 528 (1980).

[50] D. Poenaru, W. Greiner, K. Depta, M. Ivascu, D. Mazilu, and A. Sandulescu, At. Data Nucl. Data Tables **34**, 423 (1986).

[51] G. Royer, R. K. Gupta, and V. Denisov, Nucl. Phys. A **632**, 275 (1998).

[52] D. N. Poenaru, R. A. Gherghescu, and W. Greiner, Phys. Rev. Lett. **107**, 062503 (2011).

[53] D. N. Poenaru, R. A. Gherghescu, and W. Greiner, Phys. Rev. C **85**, 034615 (2012).

[54] D. N. Poenaru, R. A. Gherghescu, and W. Greiner, J. Phys. Conf. Ser. **436**, 012056 (2013).

[55] D. N. Poenaru, R. A. Gherghescu, W. Greiner, and N. S. Shakib, "How rare is cluster decay of superheavy nuclei?" in *Nucl. Phys. Present Futur.* (Springer International Publishing, Cham, 2015) pp. 131–140.

[56] D. N. Poenaru and R. A. Gherghescu, Phys. Rev. C **97**, 044621 (2018).

[57] K. P. Santhosh and C. Nithya, Phys. Rev. C **97**, 064616 (2018).

[58] Y. L. Zhang and Y. Z. Wang, Phys. Rev. C **97**, 014318 (2018).

[59] M. Warda and L. M. Robledo, Phys. Rev. C **84**, 044608 (2011), arXiv:1107.1478 .

[60] M. Warda, A. Zdeb, and L. M. Robledo, Phys. Rev. C **98**, 041602 (2018).

[61] D. N. Poenaru and W. Greiner, "Cluster radioactivity," in *Clust. Nucl. Vol. 1*, edited by C. Beck (Springer Berlin Heidelberg, Berlin, Heidelberg, 2010) pp. 1–56.

[62] H. J. Rose and G. A. Jones, Nature **307**, 245 (1984).

[63] A. Staszczak, A. Baran, and W. Nazarewicz, Phys. Rev. C **87**, 024320 (2013), arXiv:arXiv:1208.1215v1 .

[64] A. Baran, M. Kowal, P.-G. Reinhard, L. M. Robledo, A. Staszczak, and M. Warda, Nucl. Phys. A **944**, 442 (2015), arXiv:1503.01608 .

[65] N. T. Brewer, V. K. Utyonkov, K. P. Rykaczewski, Y. T. Oganessian, F. S. Abdullin, R. A. Boll, D. J. Dean, S. N. Dmitriev, J. G. Ezold, L. K. Felker, R. K. Grzywacz, M. G. Itkis, N. D. Kovrizhnykh, D. C. McInturff, K. Miernik, G. D. Owen, A. N. Polyakov, A. G. Popeko, J. B. Roberto, A. V. Sabel'nikov, R. N. Sagaidak, I. V. Shirokovsky, M. V. Shumeiko, N. J. Sims, E. H. Smith, V. G. Subbotin, A. M. Sukhov, A. I. Svirikhin, Y. S. Tsyganov, S. M. Van Cleve, A. A. Voinov, G. K. Vostokin, C. S. White, J. H. Hamilton, and M. A. Stoyer, Phys. Rev. C **98**, 024317 (2018).

[66] S. A. Giuliani, L. M. Robledo, and R. Rodríguez-Guzmán, Phys. Rev. C **90**, 054311 (2014).

[67] J. Sadhukhan, J. Dobaczewski, W. Nazarewicz, J. A. Sheikh, and A. Baran, Phys. Rev. C **90**, 061304 (2014), arXiv:arXiv:1410.1264v1 .

[68] P.-H. Heenen, J. Skalski, A. Staszczak, and D. Vretenar, Nucl. Phys. A **944**, 415 (2015).

[69] S. A. Giuliani, Z. Matheson, W. Nazarewicz, E. Olsen, P.-G. Reinhard, J. Sadhukhan, B. Schuetrumpf, N. Schunck, and P. Schwerdtfeger, Rev. Mod. Phys. **91**, 011001 (2019).

[70] J. Randrup, P. Möller, and A. J. Sierk, Phys. Rev. C **84**, 034613 (2011).

[71] A. J. Sierk, Phys. Rev. C **96**, 034603 (2017), arXiv:1711.02234 .

[72] Y. T. Oganessian, V. K. Utyonkov, Y. V. Lobanov, F. S. Abdullin, A. N. Polyakov, R. N. Sagaidak, I. V. Shirokovsky, Y. S. Tsyganov, A. A. Voinov, G. G. Gulbekian, S. L. Bogomolov, B. N. Gikal, A. N. Mezentsev, S. Iliev, V. G. Subbotin, A. M. Sukhov, K. Subotic, V. I. Zagrebaev, G. K. Vostokin, M. G. Itkis, K. J. Moody, J. B. Patin, D. A. Shaughnessy, M. A. Stoyer, N. J. Stoyer, P. A. Wilk, J. M. Kenneally, J. H. Landrum, J. F. Wild, and R. W. Lougheed, Phys. Rev. C **74**, 044602 (2006).

[73] Y. Oganessian, V. Utyonkov, Y. Lobanov, F. Abdullin, A. Polyakov, I. Shirokovsky, Y. Tsyganov, G. Gulbekian, S. Bogomolov, B. Gikal, A. Mezentsev, S. Iliev, V. Subbotin, A. Sukhov, A. Voinov, G. Buklanov, K. Subotic, V. Zagrebaev, M. Itkis, J. Patin, K. Moody, J. Wild, M. Stoyer, N. Stoyer, D. Shaughnessy, J. Kenneally, and R. Lougheed, Nucl. Phys. A **734**, 109 (2004).

[74] M. Arnould, S. Goriely, and K. Takahashi, Phys. Rep. **450**, 97 (2007).

[75] J. Beun, G. C. McLaughlin, R. Surman, and W. R. Hix, Phys. Rev. C **77**, 035804 (2008).

[76] S. Goriely, Eur. Phys. J. A **51**, 22 (2015).

[77] M. Eichler, A. Arcones, A. Kelic, O. Korobkin, K. Langanke, T. Marketin, G. Martinez-Pinedo, I. Panov, T. Rauscher, S. Rosswog, C. Winteler, N. T. Zinner, and F.-K. Thielemann, Astrophys. J. **808**, 30 (2015).

[78] N. Vassh, R. Vogt, R. Surman, J. Randrup, T. M. Sprouse, M. R. Mumpower, P. Jaffke, D. Shaw, E. M. Holmbeck, Y.-L. Y. Zhu, Others, and G. C. Mclaughlin, , 1 (2018), arXiv:1810.08133 [nucl-th] .

[79] N. Schunck, D. Duke, H. Carr, and A. Knoll, Phys. Rev. C **90**, 054305 (2014), arXiv:1311.2616 .

[80] N. Schunck, D. Duke, and H. Carr, Phys. Rev. C **91**, 034327 (2015), arXiv:1311.2620 .

[81] Y. Zhu, R. T. Wollaeger, N. Vassh, R. Surman, T. M. Sprouse, M. R. Mumpower, P. Möller, G. C. McLaughlin, O. Korobkin, T. Kawano, P. J. Jaffke, E. M. Holmbeck, C. L. Fryer, W. P. Even, A. J. Couture, and J. Barnes, Astrophys. J. **863**, L23 (2018).

[82] R. Brandt, S. G. Thompson, R. C. Gatti, and L. Phillips, Phys. Rev. **131**, 2617 (1963).

[83] W. Younes and D. Gogny, Phys. Rev. C **80**, 054313 (2009), arXiv:0910.1284 .

[84] W. Younes and D. Gogny, Phys. Rev. Lett. **107**, 132501 (2011), arXiv:1103.3466 .

[85] A. L. Goodman, Nucl. Phys. A **352**, 30 (1981).

[86] M. Baranger and M. Véneroni, Ann. Phys. (N. Y). **114**, 123 (1978).